AN ELECTRONIC BAND STRUCTURE STUDY

OF TTF-TCNQ AND (SN)x

by

WALDEMAR ISEBRAND FRIESEN

B.Sc., Brock University, 1973

A THESIS SUBMITTED IN PARTIAL FULFILMENT OF

THE REQUIREMENTS FOR THE DEGREE OF

MASTER OF SCIENCE

in the Department

of

PHYSICS

We accept this thesis as conforming to the

required standard

THE UNIVERSITY OF BRITISH COLUMBIA

October, 1975

In presenting this thesis in partial fulfilment of the requirements for
an advanced degree at the University of British Columbia, I agree that
the Library shall make it freely available for reference and study.
I further agree that permission for extensive copying of this thesis
for scholarly purposes may be granted by the Head of my Department or
by his representatives. It is understood that copying or publication
of this thesis for financial gain shall not be allowed without my
written permission.

Department of ___PHYSICS_____

The University of British Columbia
2075 Wesbrook Place
Vancouver, Canada
V6T 1W5

Date ___Oct. 8, 1975_____

Abstract

The electronic energy band structures of two highly conducting, anisotropic solids have been calculated using the extended Hückel method. One-, two-, and three-dimensional models of the organic charge transfer salt tetrathiofulvalinium tetracyanoquinodimethan (TTF-TCNQ) and of the inorganic polymer polysulphur nitride (SN)x have been studied.

The results indicate that the band structure of TTF-TCNQ is well described by a tight-binding, one-dimensional model in which interactions between stacks of molecules are neglected. The Fermi surface is seen to consist of extremely flat electron and hole surfaces, the nature of which is inconclusive in predicting a Fermi-surface-related instability leading to a Peierls distortion.

A one-dimensional model of (SN)x predicts metallic behaviour as the Fermi energy is found to lie at a symmetry-induced point of degeneracy where two bands cross. The single chain is highly unstable against a symmetry-reducing distortion; however, three-dimensional interchain inter-actions appear to stabilize the structure. Consequently, the Fermi surface is that of a semimetal with electron and hole pockets. The essential features of the band structure can be explained by a simple tight-binding model involving SN molecular anti-bonding π orbitals. Differences in the reported crystal structures used in the calculation are seen to have no qualitative effect.

Table of Contents

List of Tables

List of Figures

Acknowledgements

I would like to thank Dr. Birger Bergersen for introducing me to the world of one dimension, and for his subsequent patient and knowledgeable supervision. The ubiquitous and stimulating presence of Dr. John Berlinsky led to many fruitful discussions and is hereby gratefully acknowledged.

Appreciation for valuable discussions must also be expressed to the Friends of TCNQ, Dr. Jim Carolan, Dr. Dan Litvin, Tom Tiedje, and Dr. Larry Weiler, and to Dr. T.M. Rice. I thank Dr. Gilbert Lonzarich for the use of his Fermi surface plotting program.

The members of the West Penthouse also deserve a word of appreciation for their constant encouragement and moral support.

Finally,I am grateful to the National Research Council for their financial assistance in the form of a Postgraduate Scholarship.

Chapter 1: Quasi-One-Dimensional Metals

1.1 Introduction

One of the most significant developments in solid state physics in recent years has been the dicovery that certain organic solids with a high degree of anisotropy exhibit metallic properties. The importance of these "quasi-one-dimensional" materials is that they provide a direct experimental check of the theory which has been worked out for various one-dimensional (1-D) models.

Of particular interest are the charge transfer salts of tetracyano-quinodimethan (TCNQ) which have the highest electrical conductivity of any known organic salts. The large planar TCNQ molecule is a good acceptor with the extra electron occupying, unpaired, a π-orbital (i.e. a wavefunction which is odd under reflection through the molecular plane). This feature, together with the arrangement of the molecules face-to-face in stacks imparts a strong 1-D character to the electronic properties.

An impetus to the research effort in this field was provided by Coleman et al. (1973) who reported measurements on tetrathiofulvalinium tetracyanoquinodimethan (TTF-TCNQ). They observed a metallic conductivity from room temperature down to 58K where it became anomalously high, or in their words, superconducting. Below 58K, a sharp drop in the conductivity indicating a phase transition to an insulating state was observed. Further work by various groups has confirmed the metallic properties and the metal-insulator transition, but has not duplicated the extremely high conductivity. The work on TTF-TCNQ has spawned a whole host of organic solids with similar properties; however, TTF-TCNQ remains the prototype, and

consequently the most studied.

A good deal of the interest in 1-D conductors stems from the concept of a high temperature superconductor first introduced by Little (1964). While attention has been focussed on the TCNQ salts in this regard, other quasi-1-D systems have also been investigated. One, the inorganic polymer polysulphur nitride ((SN)x) which was known to have a high conductivity, has recently been shown by Greene et al. (1975) to undergo a superconducting transition at about 0.3K. (SN)x is, in some respects, quite similar to TTF-TCNQ; it differs, though, in that it does not have a metal-insulator transition.

Superconducting or not, quasi-1-D materials are of fundamental interest as novel, relatively unstudied systems. This thesis concerns itself with a study of the two different examples already mentioned, TTF-TCNQ and (SN)x. Some experimental results and several theoretical concepts are presented in the remainder of this chapter. Chapter 2 deals with TTF-TCNQ and Chapter 3 with (SN)x. Finally, in Chapter 4, the results of the calculations are discussed, and a comparison of the two systems is made.

1.2 TTF-TCNQ: An Organic Metal

In TTF-TCNQ the two constituent molecules are stacked on separate chains which interact weakly in comparison to the intrachain coupling, resulting in conduction primarily along the chain axis. Because TTF is a good donor, a charge of $\sim$ one electron per TTF is transferred to the TCNQ. Each chain thus carries a net charge so that in a simple 1-D band picture TTF-TCNQ is expected to be a metal.

Typical room temperature conductivities parallel to the chain axis

are $\sigma_{RT}^{\parallel} \sim 300 - 1000 \ (\Omega\text{-cm})^{-1}$ (Tiedje, 1975; Schafer et al., 1974;
Etemad et al.,1975). As the temperature is lowered, $\sigma^{\parallel}$ increases approx-
imately as T^{-2} to a peak value of $10 - 15 \ \sigma_{RT}^{\parallel}$. At 53K, a sudden drop occurs,
signifying a phase transition to semiconducting state. Below 53K, $\sigma^{\parallel}$
decreases smoothly down to 38K, where another sharp drop occurs, marking
another phase transition. The room temperature transverse conductivity,
$\sigma_{RT}^{\perp}$, is only about 1.4 $(\Omega\text{-cm})^{-1}$ with a 58K peak of three times this figure.
The anisotropy $\sigma^{\parallel}/\sigma^{\perp}$ is thus greater than 300.

Various other experiments have confirmed one or both transitions:
magnetoresistance (Tiedje et al.,1975), thermal conductivity (Salamon et
al., 1975), specific heat (Craven et al., 1974), magnetic susceptibility
(Tomkiewicz et al., 1974), and the thermoelectric power (Chaikin et al.,
1973). The experimental conclusion is that TTF-TCNQ is a metal above 53K
and a small gap semiconductor below.

1.3 (SN)x: A Polymeric Superconductor

(SN)x has been known to be highly conducting since the experiments
of Goehring (1956). It is only with the recent interest in the quasi-1-D
solids that (SN)x has again become subject to experiment. The structure
is similar to that of TTF-TCNQ, consisting of parallel chains of atoms.
The room temperature conductivity parallel to the chain direction is
$\sigma_{RT}^{\parallel} \sim 1000 \ (\Omega\text{-cm})^{-1}$ (Hsu and Labes, 1974; Greene et al., 1975); with de-
creasing temperature $\sigma^{\parallel}$ increases until the onset of superconductivity
at 0.26K. The transverse conductivity, $\sigma^{\perp}$, is much lower, the anisotropy
$\sigma^{\parallel}/\sigma^{\perp}$ ranging from 50 - 1000. It should be stressed that no metal-
insulator transition is observed. An important feature of the macroscopic
crystal structure relevant to any discussion of the anisotropy is the

crystallization of (SN)x into "bundles of fibers", with fiber diameters of about 1000 Å. The effect of this fibrous structure on the transverse properties is not clear.

1.4 One-Dimensional Theories

The phrase "one-dimensional metal" is in one sense a paradox, since a 1-D non-interacting electron gas in a periodic potential cannot be a conductor. This was shown by Peierls (1955), and can be illustrated by a simple example which is sketched in Fig. 1. Consider a chain of atoms with one atom per unit cell, and lattice spacing a; if, in the tight-binding approximation, each atom contributes one electron to the conduc-tion band, the band is exactly half-filled, with Fermi wavevector $k_F = \pi/2a$. In this case the band is clearly metallic. However, a dimer-ization of the chain reduces the symmetry by doubling the lattice spacing to 2a, which shifts the Brillouin Zone boundary to $k = k_F$. A gap opens up at k_F, thereby reducing the electronic energy and making the metallic chain unstable against such a periodic deformation, or Peierls distortion, of wavevector $q = 2k_F$. This instability is not confined to a half-filled band, but will occur for any degree of band-filling.

When electron-phonon interactions are included, the same symmetry-reducing transition may occur as the manifestation of an effect first predicted by Kohn (1959). Physically this effect arises from the fact that electrons near the Fermi surface with $\vec{k} \simeq \vec{k}_F$ can be scattered in an energy conserving process by phonons with wavevector $\vec{q} = -2\vec{k}$. As $\vec{k} \to \vec{k}_F$, the first derivative of the dielectric function diverges, reflecting a sudden change in the ability of the electron gas to screen the lattice
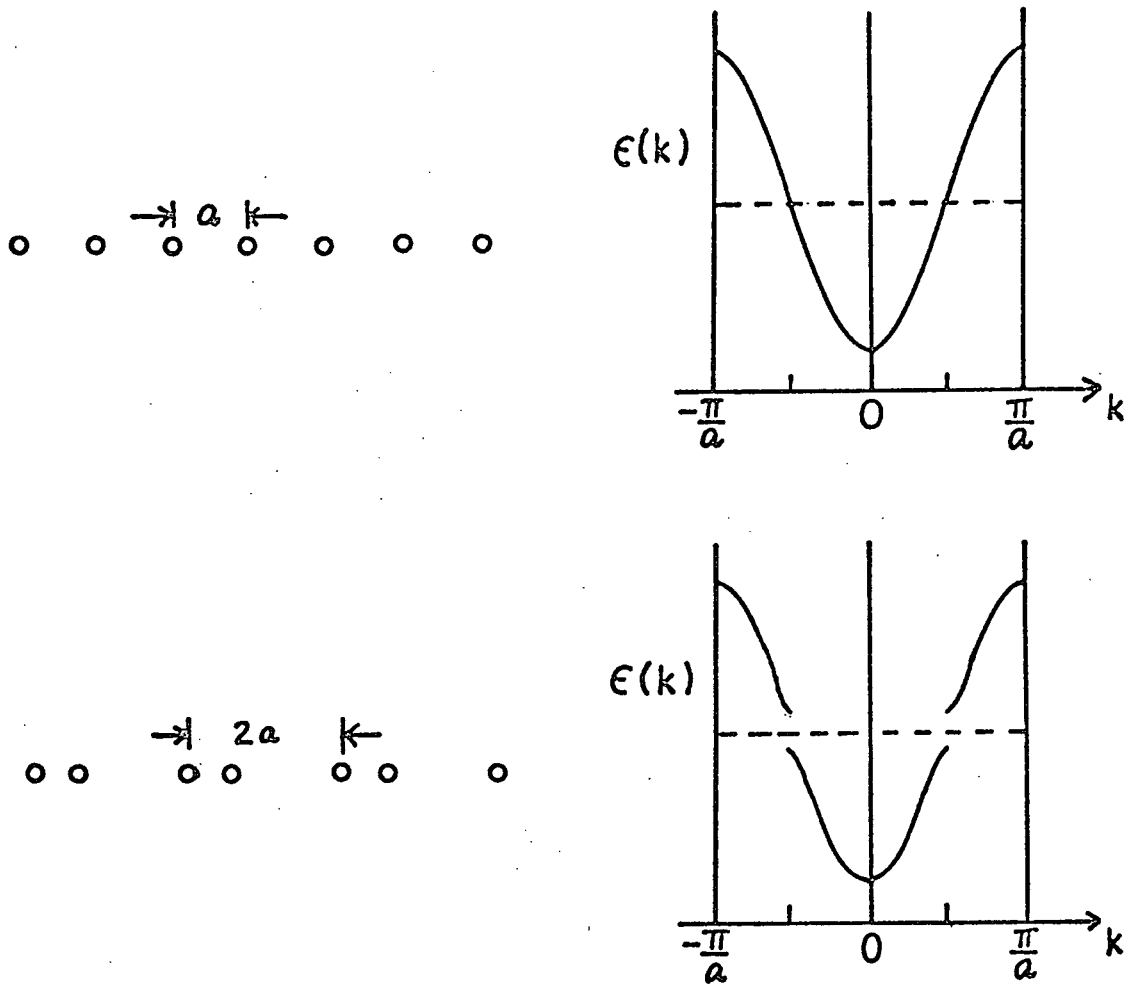
Figure 1. Effect of a Peierls distortion. (a) Tight-binding energy band for the linear chain with interatomic spacing a. (b) The bands for the chain in which the atoms have dimerized to double the lattice parameter to 2a.

vibration. The resultant kink in the phonon energy is known as the Kohn anomaly. In the case when the phonon frequency goes to zero, the lattice vibration becomes a permanent (Peierls) distortion with wavevector $2\vec{k}_F$. The strength of the effect depends on how much of the Fermi surface can be connected by the wavevector $2\vec{k}_F$ (or how well the Fermi surface nests). In 2- or 3-D, the effect is a weak one; in 1-D however, the anomaly is

pronounced since the Fermi surface consists of two singular points at k_F, and the nesting is perfect.

A discussion of the Fermi surface instability within mean field theory has been given by Rice and Strässler (1973). They consider a linear chain with a half-filled tight-binding band. The (Fröhlich) Hamiltonian is written as,

$$H = \sum_p \varepsilon_p c_p^+ c_p + \sum_q \hbar \omega_q b_q^+ b_q + \frac{1}{\sqrt{N}} \sum_p \sum_q g(q) c_{p+q}^+ c_p (b_q + b_{-q}^+) \tag{1}$$

Here the b's and c's are the usual operators for the unperturbed phonons of energy $\hbar \omega_q$ and Bloch electrons of energy ε_p respectively; N is the number of ions in the chain, and g(q) is the electron-phonon coupling constant. The screened phonon frequencies, Ω_q, of the coupled electron-phonon system are given by,

$$\Omega_q^2 = \omega_q^2 - \chi(q,T) g^2(q) \tag{2}$$

where the susceptibility $\chi(q,T)$ is defined as,

$$\chi(q,T) = \frac{\omega_q}{N\hbar} \sum_p \frac{f_p - f_{p-q}}{\varepsilon_{p-q} - \varepsilon_p} \tag{3}$$

f_p is the Fermi distribution function.

Defining a dimensionless parameter $\lambda = \hbar \omega_{q_0} / 2g^2 N(0)$ in which g = $g(q_0 = 2k_F)$ and N(0) is the density of states at the Fermi level, the phonon frequency Ω_{q_0} is found to be,

$$\Omega_{q_0} = \left(\frac{\omega_{q_0}^2}{2\lambda} \right) \ln \left(\frac{T}{T_c} \right) \tag{4}$$

where

$$kT_c = 2.28 \, \varepsilon_F \, e^{-2\lambda} \tag{5}$$

Thus Ω_{q_0} approaches zero logarithmically as T approaches the critical temperature T_c.

Below T_c, Rice and Strässler view the linear chain as a condensed phonon state of wavevector q_0 such that the expectation values $\langle b_q \rangle = \langle b_q^\dagger \rangle = (Nu/2)\delta_{q,q_0}$, where u is a dimensionless amplitude. In this case an energy gap of magnitude $2\Delta(T)$ appears in the electronic energy spectrum at $p = k_F$. From a zero temperature value $\Delta(0) = 4\varepsilon_F e^{-2\lambda}$, the gap decreases, vanishing finally at the T_c given by (5). In the framework of this model, then, the high temperature metal undergoes a second order phase transition to a low temperature insulator.

It has been argued that the Kohn anomaly does not always lead to an insulating state. Fröhlich (1954) considered a system with the Hamiltonian given by (1) and argued that superconductivity might result in the following manner. When an external field is applied the electrons are displaced in k-space with a velocity v_s. If the macroscopically occupied lattice vibration with wavevector $2k_F$ moves with the electrons, a super-lattice of periodicity $2\pi/2k_F$ exists in the frame of the electrons. Consequently, energy gaps will appear at the displaced Fermi surface as in Fig. 2.

At low temperatures the lower band is completely filled, and as long as the two bands do not overlap no scattering can occur; this gives rise to a supercurrent. In the crystal frame the electronic energy is $E(k) + \hbar k_F v_s$. When $\hbar k_F v_s$ becomes greater than half the gap, Δ, the free energy is lowered by electrons being scattered into the conduction band, thereby introducing a resistance and decreasing the supercurrent. The coupled electron-phonon mode described here is known as a Fröhlich mode. Bardeen (1973) has suggested that the Fröhlich mode might be a mechanism
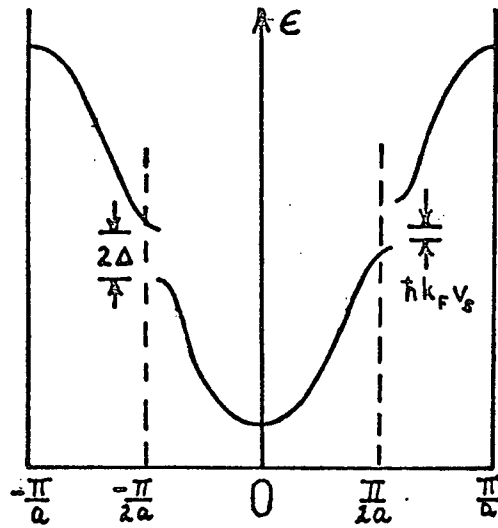
Figure 2. Shift of the electronic energy gap in an electric field
when the lattice distortion moves with the current.

for the high conductivity in TTF-TCNQ.

Unfortunately, mean field theory is inaccurate in describing 1-D
systems due to fluctuations of the order parameter. Landau and Lifshitz
(1969) have shown that for a system with short range forces, fluctuations
prohibit a phase transition except at zero temperature.

Lee, Rice, and Anderson (1973) have included fluctuations in a 1-D
model using the correlation length, ξ, as the order parameter in a genera-
lized Landau theory. They find that for $T \lesssim T_c$ (T_c being the mean field
transition temperature), $\xi(T)$ becomes large, increasing exponentially
with temperature. Although $\xi(T)$ diverges only at $T = 0$, it is large
enough so that with a weak 3-D coupling a 3-D transition can occur at
$T \simeq 1/4\ T_c$. The effect of the fluctuations on the electronic density of
states is to change the well-defined gap which exists at $T = 0$ to a
"pseudo-gap"; that is, an energy interval in which the density of states
is nearly zero. This result would then have some influence on the Kohn
anomaly.

One-dimensional models are unrealistic in the sense that they ignore the finite, if small, interchain interactions that are present in real systems. Horovitz, Gutfreund, and Weger (HGW,1975) have included interchain effects in the model described by (1) with nearest-neighbour tight-binding of the form,

$$\mathcal{E}(p_y) = -\mathcal{E}_F \cos p_y c$$
$$\simeq \mathcal{E}_o \left[\pm \frac{2 \delta p_y}{p_F} + \alpha \left(\frac{\delta p_z}{p_F} \right)^2 \right] \; ; \; \delta p_z = \mp p_F \; \text{for} \; p_z \lessgtr 0$$

$$(6)$$

parallel to the chain, and

$$\mathcal{E}(p_x, p) \equiv \mathcal{E}(p_\perp) = -\eta \, \mathcal{E}_o \left(\cos a p_x + \cos a p_z \right) \tag{7}$$

transverse to the chain. Here ϵ_F, p_F are the Fermi energy and wavevector for a single chain, ϵ_o is an energy parameter $\simeq \epsilon_F$, η is the ratio of the interchain to the intrachain coupling ($\eta \ll 1$), and α is a measure of the band-filling. For a half-filled band ($\alpha = 0$) the Fermi surface appears effectively flat to the wavevector $\vec{q}_o = (\pi/a, 2p_F, \pi/a)$; that is to say, the Fermi wavevector nests perfectly for $\vec{q}_o$. This implies a giant Kohn amomaly at $\vec{q}_o$. When the band is other than half-filled, the wavevectors connecting the Fermi surface do not have the same q_b component, resulting in a smearing of the Kohn anomaly. There exists a critical value η_c of the interchain coupling strength such that for $\eta > \eta_c$ the Peierls transition is suppressed; for example, at $T = 0$, $\eta_c \simeq 3.5 \sqrt{T_c(\eta=0)/\epsilon_o |\alpha|}$, T_c again denoting the mean field transition temperature. It is interesting to note that for $\alpha = 0$, the interchain coupling does not affect the instability.

A transition at $\vec{q}_1 = (0, 2p_F, 0)$ can also occur if $\eta < \eta_c' \simeq \sqrt{T_c(\eta=0)/\epsilon_o}$.

In fact, an instability will exist at any $q_\perp$ for which the electron-phonon coupling parameter $\lambda(\vec{q})$ is a maximum. If there is no strong dependence on $q_\perp$, however, the $\vec{q} = \vec{q}_o$ instability will be favoured for those values of the interchain coupling for which $\eta \gtrsim \eta_c' \simeq T_c/\epsilon_o$; it is roughly in this region that fluctuation effects are small.

When fluctuations are included in a treatment of the instability at $\vec{q}_o$, HGW find a temperature characteristic of the system, $T_b = \eta\epsilon_o/4$; for a phase transition to occur it is required that the real transition temperature be $\lesssim T_b$. Further, 1-D mean field theories are found to be appropriate in the region,

$$\frac{4}{\epsilon_o} T_c^o(\eta = 0) \lesssim \eta \lesssim 3\sqrt{\frac{T_c^o(\eta = 0)}{\epsilon_o |\alpha|}} \tag{8}$$

where T_c^o is the mean field T_c for $\vec{q} = \vec{q}_o$.

1.5 Energy Band Calculation

In this section the method used in calculating the energy bands is outlined. A linear combination of atomic orbitals (LCAO) method is used for (SN)x because of the covalent bonding nature of the constituents. The same method in which the atomic orbitals are replaced by molecular orbitals is used for TTF-TCNQ.

The electronic wavefunction, $\Psi_{\vec{k}}(\vec{r})$ is expanded as a linear combination of Bloch orbitals,

$$\Psi_{\vec{k}}(\vec{r}) = \frac{1}{\sqrt{N}} \sum_i a_i^{\vec{k}} \psi_i^{\vec{k}}(\vec{r}) \tag{9}$$

where

$$\psi_i^{\vec{k}}(\vec{r}) = \sum_m' e^{i\vec{k}\cdot\vec{R}_m} \varphi_i(\vec{r} - \vec{R}_m - \vec{r}_i) \tag{10}$$

Here $\phi_i(\vec{r} - \vec{R}_m - \vec{r}_i)$ is the i'th atomic orbital centered at position $\vec{r}_i$ in the unit cell with postion vector $\vec{R}_m$, and N is the number of unit cells in the crystal. Substitution of (9) into the Schrödinger equation leads eventually to the set of coupled linear equations,

$$\sum_j H_{ij} \, a_j^{\vec{k}} = \varepsilon(\vec{k}) \sum_j S_{ij} \, a_j^{\vec{k}}$$

$$\det | H(\vec{k}) - \varepsilon(\vec{k}) \, S(\vec{k})| = 0 \tag{11}$$

for the energies $\varepsilon(\vec{k})$ and the coefficients $a_j^{\vec{k}}$. The matrix elements H_{ij} and S_{ij} are given by,

$$H_{ij}(\vec{k}) = \sum_m e^{i\vec{k}\cdot\vec{R}_m} \langle \varphi_i(\vec{r}+\vec{R}_m-\vec{r}_i)| H | \varphi_j(\vec{r}-\vec{r}_j)\rangle$$

$$= \sum_m e^{i\vec{k}\cdot\vec{R}_m} h_{ij}^m$$

$$S_{ij}(\vec{k}) = \sum_m e^{i\vec{k}\cdot\vec{R}_m} \langle \varphi_i(\vec{r}+\vec{R}_m-\vec{r}_i)| \varphi_j(\vec{r}-\vec{r}_j)\rangle \tag{12}$$

$$= \sum_m e^{i\vec{k}\cdot\vec{R}_m} s_{ij}^m$$

The integrals h_{ij}^m were calculated using the semiempirical extended Hückel method (EHM) of Hoffman (1963). In this approximation the term h_{ij}^m is scaled with the overlap s_{ij}^m as follows:

$$h_{ij}^m = \begin{cases} \varepsilon_i & \text{if } i=j, m=0 \\ \frac{1}{2} K(\varepsilon_i + \varepsilon_j) s_{ij}^m & \text{otherwise} \end{cases} \tag{13}$$

K is the phenomenological Wolfsberg-Helmholtz parameter which is varied to give the best fit to experiment. Usually K is taken to be 1.75, a value which was used in our calculation. ε_i is the experimentally deter-

mined ionization potential for orbital i. If n orbitals per unit cell are included, the energy bands are obtained by solving the n x n eigenvalue equation (11) for each wavevector.

The EHM allows the full symmetry of the crystal to be incorporated correctly. While the method is somewhat crude, it is expected to give energy differences such as bandwidths quite well. In addition, its simplicity leads to an easy interpretation of the energy eigenvectors. The EHM has been used in similar calculations by several authors: M[c]Cubbin and Manne (1968) and Fleming and Falk (1973) for polyethylene, Kortela and Manne (1974) for graphite, and Berlinsky et al. (1974) for TTF-TCNQ.

Chapter 2: TTF-TCNQ

2.1 Crystal Structure

The crystal structure as reported by Kistenmacher et al. (1974) is shown in Fig. 3; molecular coordinates are given in table 1. The dominant feature is the segregated chains of TTF and TCNQ molecules stacked in a monoclinic lattice. Neighbouring chains along the c-axis are related by a screw axis symmetry operation: a rotation of 180° about an axis midway between the chains, together with a translation of b/2 along the axis takes one chain into the other. A unit cell thus contains two TTF and two TCNQ molecules. The space group of the structure is $P2_1/c$, the symmetry elements of which are a center of inversion at each molecular site and the screw axis.

2.2 One-Dimensional TTF-TCNQ

The stacking arrangement of the structure, together with the observed anisotropy in the conductivity point to a model in which there are interactions only along the chain and not between the chains. That this first approximation is indeed a good one is borne out later when interchain coupling is taken into account.

A part of this section is based on the work of Berlinsky, Carolan and Weiler (BCW, 1974) since it is a necessary prelude to what follows. BCW have used the EHM to calculate the molecular orbitals (MO's) for both TTF^+ and $TCNQ^-$ molecules, with the result that the highest occupied MO on each molecule is a π-orbital. The symmetry of these MO's is such that the TTF^+ wavefunction is even and the $TCNQ^-$ wavefunction odd under
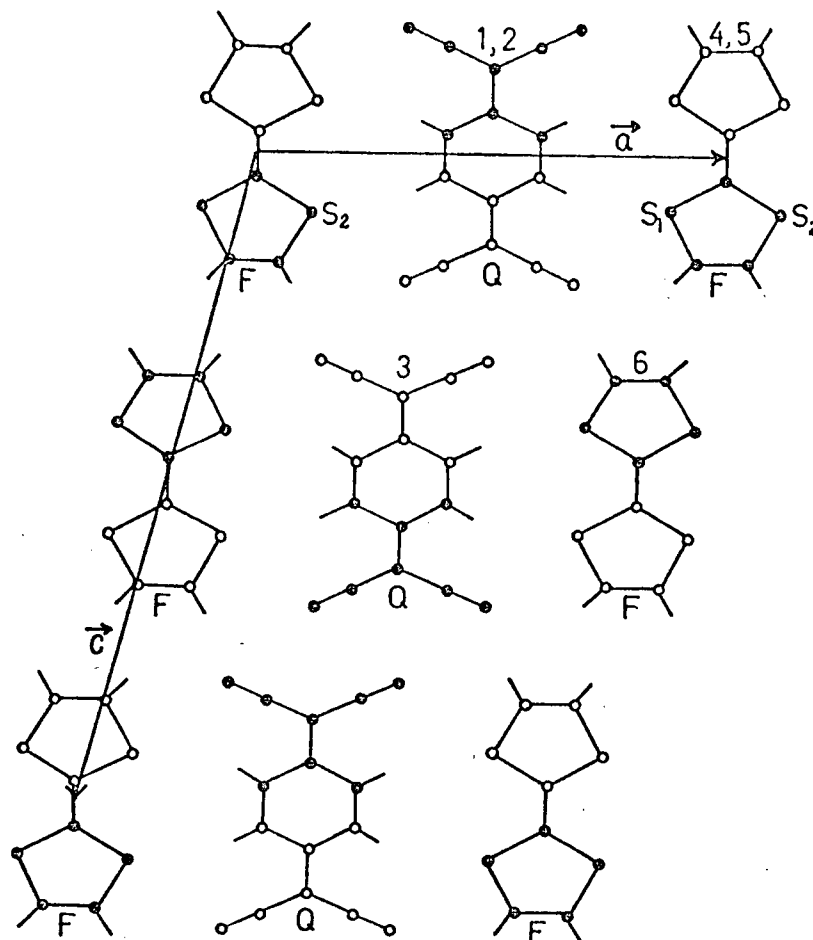
(a)
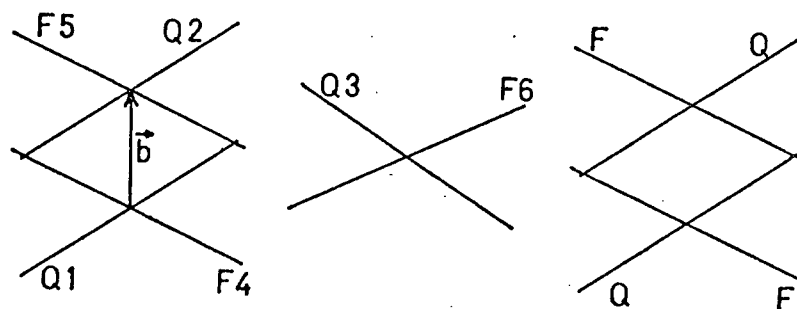
(b)

Figure 3. Crystal structure of TTF-TCNQ. TTF and TCNQ are labelled F and Q respectively, while the numbers indicate those molecules whose coordinates are given in Table 1; 1,3,4,6 are in the same unit cell and 2 and 5 are in the cell displaced by $\vec{b}$. (a) View perpendicular to the chain axis. The solid circles indicate those atoms positioned above a plane which passes through the center of the molecule and which is parallel to the $\vec{a}$-$\vec{c}$ plane. (b) Side view along the a-axis.

reflection through planes bisecting the molecules along their short dimension and normal to the molecular plane. An important consequence of this result is that the TTF-TCNQ overlap along the a-axis is identically zero, thus greatly diminishing interchain effects. Following the BCW argument that it is valid to identify these MO's with the valence and conduction bands in the solid, we take them as the basis functions for our energy band calculation. It should be pointed out that the a-axis overlap is zero only for those wavefunctions calculated for isolated molecules. Inclusion of the crystal field reduces the MO symmetry, resulting in a finite overlap. This can be seen in Fig. 3 where the atoms marked S_1 and S_2 are situated in different environments. The size and effect of a non-zero a-axis overlap is not known.

In the 1-D approximation, the calculation reduces to that for the linear atomic chain of lattice constant b and one orbital per unit cell. We write the wavefunction as,

$$\Psi_k^i(\vec{r}) = \frac{1}{\sqrt{N}} \sum_n e^{iknb} \varphi_i(\vec{r} - n\vec{b})$$

(14)

where N is the number of molecules in the chain and $\phi_i(\vec{r} - n\vec{b})$ is an MO centered at the n'th site. The subscript i = F or Q, which will hereafter denote TTF and TCNQ respectively. The energy for band i is then given by,

$$\mathcal{E}_i = \frac{\sum_m \sum_n e^{i(n-m)kb} \langle \varphi_i(\vec{r} - m\vec{b}) | H | \varphi_i(\vec{r} - n\vec{b}) \rangle}{\sum_m \sum_n e^{i(n-m)kb} \langle \varphi_i(\vec{r} - m\vec{b}) | \varphi_i(\vec{r} - n\vec{b}) \rangle}$$

(15)

Including only nearest-neighbour interactions gives,

$$\varepsilon_i = \frac{\langle \varphi_i(\vec{r})|H|\varphi_i(\vec{r})\rangle + 2\cos kb \langle \varphi_i(\vec{r}+\vec{b})|H|\varphi_i(\vec{r})\rangle}{1 + 2\cos kb \langle \varphi_i(\vec{r}+\vec{b})|\varphi_i(\vec{r})\rangle} \qquad (16)$$

Since $\langle \phi_i(\vec{r} + \vec{b})|\phi_i(\vec{r})\rangle \equiv \sigma_i \ll 1$, the denominator can be expanded to get,

$$\varepsilon_i = \left\{\langle \varphi_i(\vec{r})|H|\varphi_i(\vec{r})\rangle + 2\cos kb \langle \varphi_i(\vec{r}+\vec{b})|H|\varphi_i(\vec{r})\rangle\right\}\left\{1 - 2\sigma_i \cos kb\right\} \qquad (17)$$

Making use of the Hückel approximation and retaining only terms to first order in σ_i, we finally have,

$$\varepsilon_i = \varepsilon_i^o + 2t_i \cos kb \qquad (18)$$

where ε_i^o is the ionization potential of molecule i, and $t_i = (K - 1)\varepsilon_i^o\sigma_i$. The Fermi level intersects both bands, with the consequence that the Fermi wavevector determines the amount of filling of each band, or equivalently, the degree of charge transfer. Grobman et al. (1974) interpreted their photoemission data as indicating a charge transfer of about one electron per TTF donor. If this is the case the band is half-filled and $\varepsilon_F^o = \varepsilon_Q^o$. All calculations were therefore initially performed for a half-filled band model. Using the BCW estimate that $\varepsilon_F^o = -7.5$ eV, together with the calculated overlap integrals $\sigma_F = -9.3 \times 10^{-3}$ and $\sigma_Q = 2.0 \times 10^{-2}$, one obtains $t_F = 0.05$ eV and $t_Q = -0.11$ eV, or bandwidths of 0.20 and 0.44 eV for the F and Q bands. The fact that t_F and t_Q are opposite in sign is significant since it means that the bands must cross, and hence interact in the presence of F-Q coupling.

More recently, evidence for a Peierls distortion has been provided by an X-ray analysis of the crystal structure by Denoyer et al. (1975). Below 40K they observe a 3-D superlattice with dimensions 2a x 3.7b x nc

(n unknown). In the context of 1-D F and Q bands the new lattice parameter 3.7b implies a Fermi wavevector $k_F = \pi/3.7b$, which corresponds to a nearly quarter-filled Q band. The ionization potentials were accordingly changed to $\varepsilon_F^O = -7.58$ eV and $\varepsilon_Q^O = -7.35$ eV. The proposed band structure is presented in Fig. 4a for an undistorted chain and in Fig. 4b for a chain with a distortion wavelength of 4b.

(a)   (b)
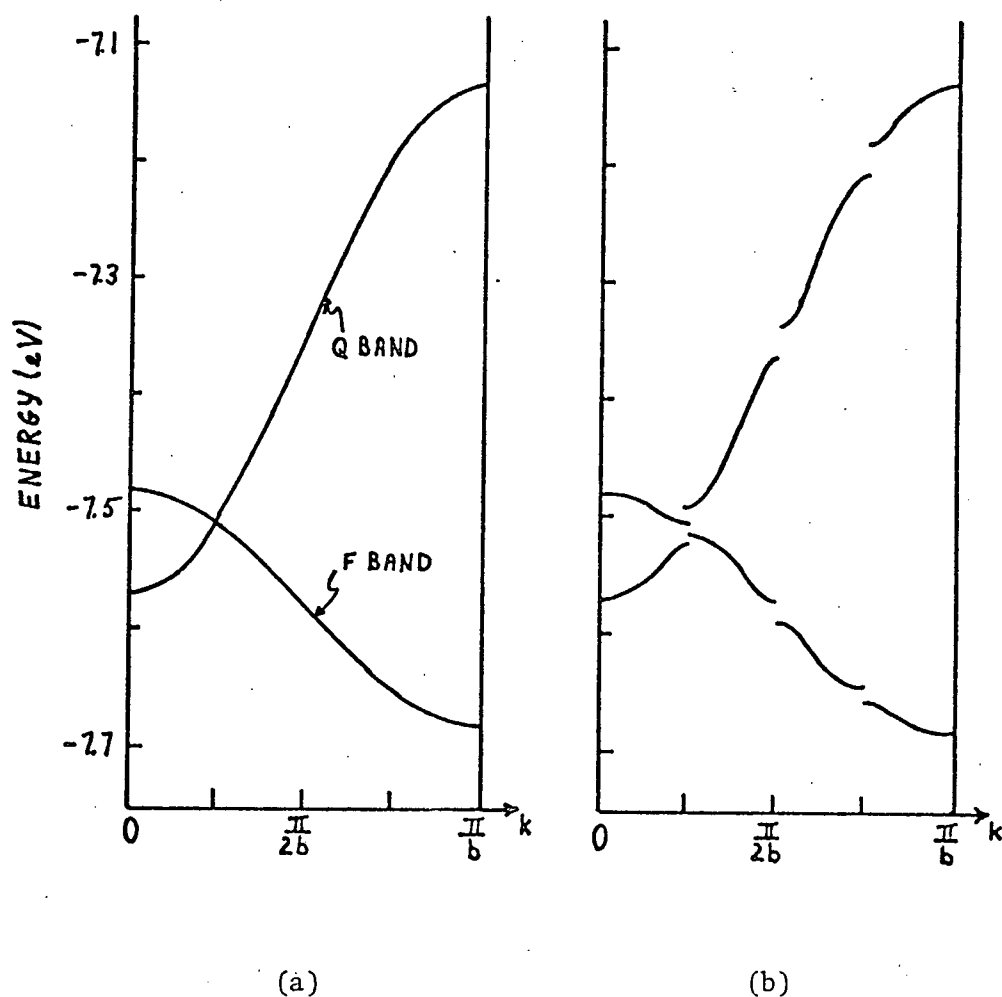
Figure 4. (a) One-dimensional energy bands for a charge transfer of 0.5 electrons per TTF molecule. (b) The effect of a Peierls distortion of wavelength 4b on the bands of (a).

The density of states for the cosine band i is, per molecule,

$$D_i(\varepsilon) = \frac{1}{\pi\sqrt{4t_i^2 - (\varepsilon - \varepsilon_i^0)^2}} \tag{19}$$

The total density of states is then simply the sum $D(\varepsilon) = D_F(\varepsilon) + D_Q(\varepsilon)$ as shown in Fig. 5.

Figure 5. Density of states for the two non-interacting bands in Fig. 4a. E_F is the Fermi energy.

2.3 Three-Dimensional TTF-TCNQ

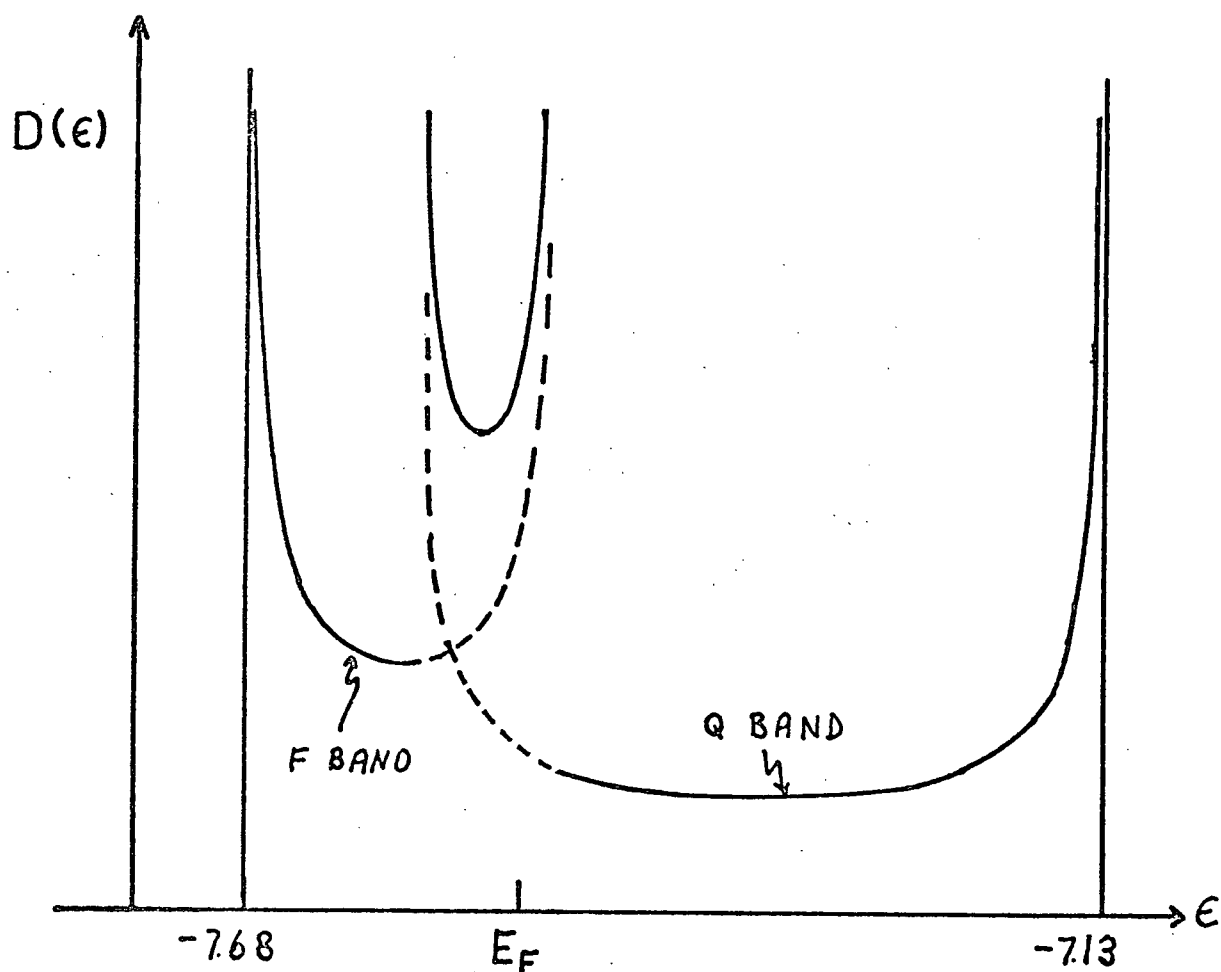Before considering the three-dimensional band structure it might be instructive to look at the 2-D case in which we include interactions between chains of like molecules. The equal-energy planes perpendicular to the b-axis of the 1-D problem disappear to be replaced by lines of equal energy normal to the b- and c-axes. Each of the doubly degenerate bands in Fig. 4a is split by the interchain coupling. The 4 x 4 secular determinant in (11) assumes a block diagonal form,

$$
\begin{vmatrix}
H_{11} - \varepsilon S_{11} & H_{12} - \varepsilon S_{12} & & \\
H_{21} - \varepsilon S_{21} & H_{22} - \varepsilon S_{22} & & 0 \\
& & H_{33} - \varepsilon S_{33} & H_{34} - \varepsilon S_{34} \\
& 0 & H_{43} - \varepsilon S_{43} & H_{44} - \varepsilon S_{44}
\end{vmatrix} = 0 \qquad (20)
$$

where, if only nearest neighbour overlaps, σ_i', on neighbouring chains are included,

$$
\begin{aligned}
S_{11} &= S_{22} = 1 + 2\sigma_F \cos \vec{k} \cdot \vec{b} \\
S_{33} &= S_{44} = 1 + 2\sigma_Q \cos \vec{k} \cdot \vec{b} \\
S_{12} &= S_{21}^* = \sigma_F' (1 + e^{-i\vec{k} \cdot \vec{c}})(1 + e^{-i\vec{k} \cdot \vec{b}}) \\
S_{34} &= S_{43}^* = \sigma_Q' (1 + e^{-i\vec{k} \cdot \vec{c}})(1 + e^{i\vec{k} \cdot \vec{b}}) \\
H_{11} &= H_{22} = \varepsilon_F^{\ o} + 2K\varepsilon_F^{\ o}\sigma_F \cos \vec{k} \cdot \vec{b} \\
H_{33} &= H_{44} = \varepsilon_Q^{\ o} + 2K\varepsilon_Q^{\ o}\sigma_Q \cos \vec{k} \cdot \vec{b} \\
H_{12} &= H_{21}^* = K\varepsilon_F^{\ o} S_{12} \\
H_{34} &= H_{43}^* = K\varepsilon_Q^{\ o} S_{34}
\end{aligned} \qquad (21)
$$

The resulting energy bands are approximately given by the expressions,

$$\mathcal{E} = \mathcal{E}_i \pm \Delta\mathcal{E}_i \; ; \tag{22}$$

where,

$$\mathcal{E}_i = \mathcal{E}_i^0 + 2(K-1)\mathcal{E}_i^0 \sigma_i \cos \vec{k} \cdot \vec{b}$$

$$\Delta\mathcal{E}_i = 4(K-1)\mathcal{E}_i^0 \sigma_i' \cos \frac{\vec{k} \cdot \vec{c}}{2} \cos \frac{\vec{k} \cdot \vec{b}}{2}$$

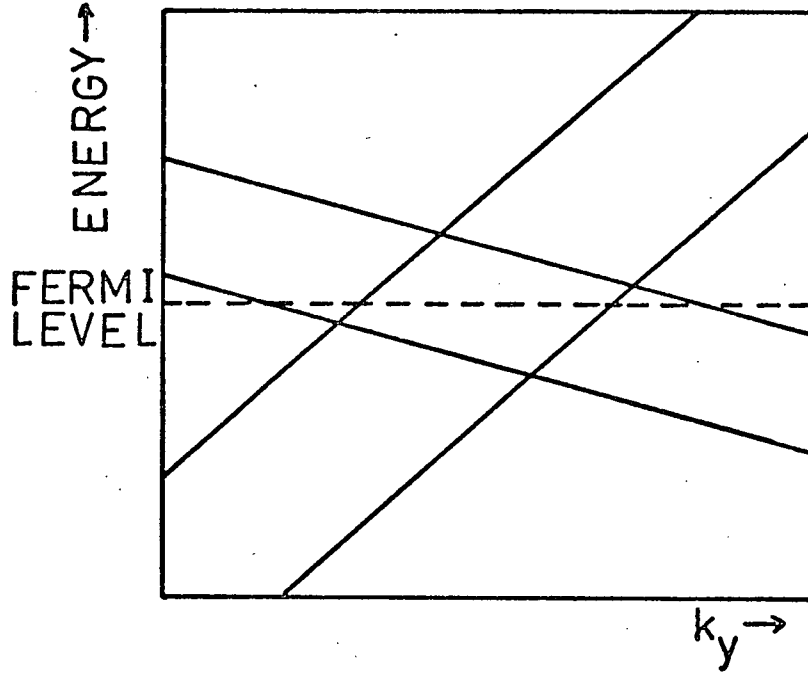In the region of the band crossing the bands will appear as in Fig. 6.

Figure 6. Energy bands along k_y in the region of the band crossing in the 2-D case.

The points at which the Fermi level intersects the bands are determined by the magnitude of the splittings E_i. Since $\sigma_i' \ll 1$, the bands are extremely flat. The deviation of the Fermi wavevector from $k_b = \pi/4b$ will then be small, wo we may write it as,

$$k_{Fb} = \frac{\pi}{b}\left(\frac{1}{4} - \beta\right), \qquad \beta \ll 1 \tag{23}$$

Using equations (22) gives,

$$(1-\beta) = \frac{0.94}{\sigma_i'}\left(\frac{E_F}{\varepsilon_i^o} - 1\right) \pm \frac{\sigma_F^2}{\sigma_F'}\cos\left(\frac{\vec{k}\cdot\vec{c}}{2}\right)\left(2.61 - 1.08\beta\right) \tag{24}$$

A cross-section of the Fermi surface in the b-c plane is sketched in Fig. 7. The surfaces have been labelled F or Q depending on which band the Fermi surface crosses. It is readily apparent as indicated by the arrows that the portion of the Fermi surface in the upper half of the zone nests perfectly with the portion in the lower half. One would thus expect the 2-D model of TTF-TCNQ as outlined here to be unstable against a distortion of wavevector $\vec{q} = (q_a, q_b, q_c) = (\pi/\alpha a, \pi/2b, 0)$, with $\alpha \approx 1$ determining the periodicity in the a-direction. From the discussion of HGW, α would be that value maximizing the electron-phonon coupling constant $\lambda(\vec{q})$.

A 2-D model for TTF-TCNQ is not really valid since the interaction energy between F and Q chains is roughly of the same magnitude as that for the F-F and Q-Q couplings. When F-Q interactions are added the degeneracies at the crossover points are lifted and some small curvature in the $\vec{a} \times \vec{c}$ direction is added to the equal energy lines. Fig. 8 indicates what happens to the bands in the crossover region in a direction parallel to the b-axis. Whether or not an energy gap occurs depends on the strength of the F-Q coupling.

The important interchain overlaps (from BCW) are presented in Table 2. With these overlaps, the terms in the secular determinant not given by (21) are,

$$S_{31} = S_{42} = S_{13}^* = S_{24}^* = \sigma_{FQ}'(e^{-i\vec{k}\cdot\vec{b}} - e^{i\vec{k}\cdot\vec{b}})(1 + e^{i\vec{k}\cdot\vec{a}})$$

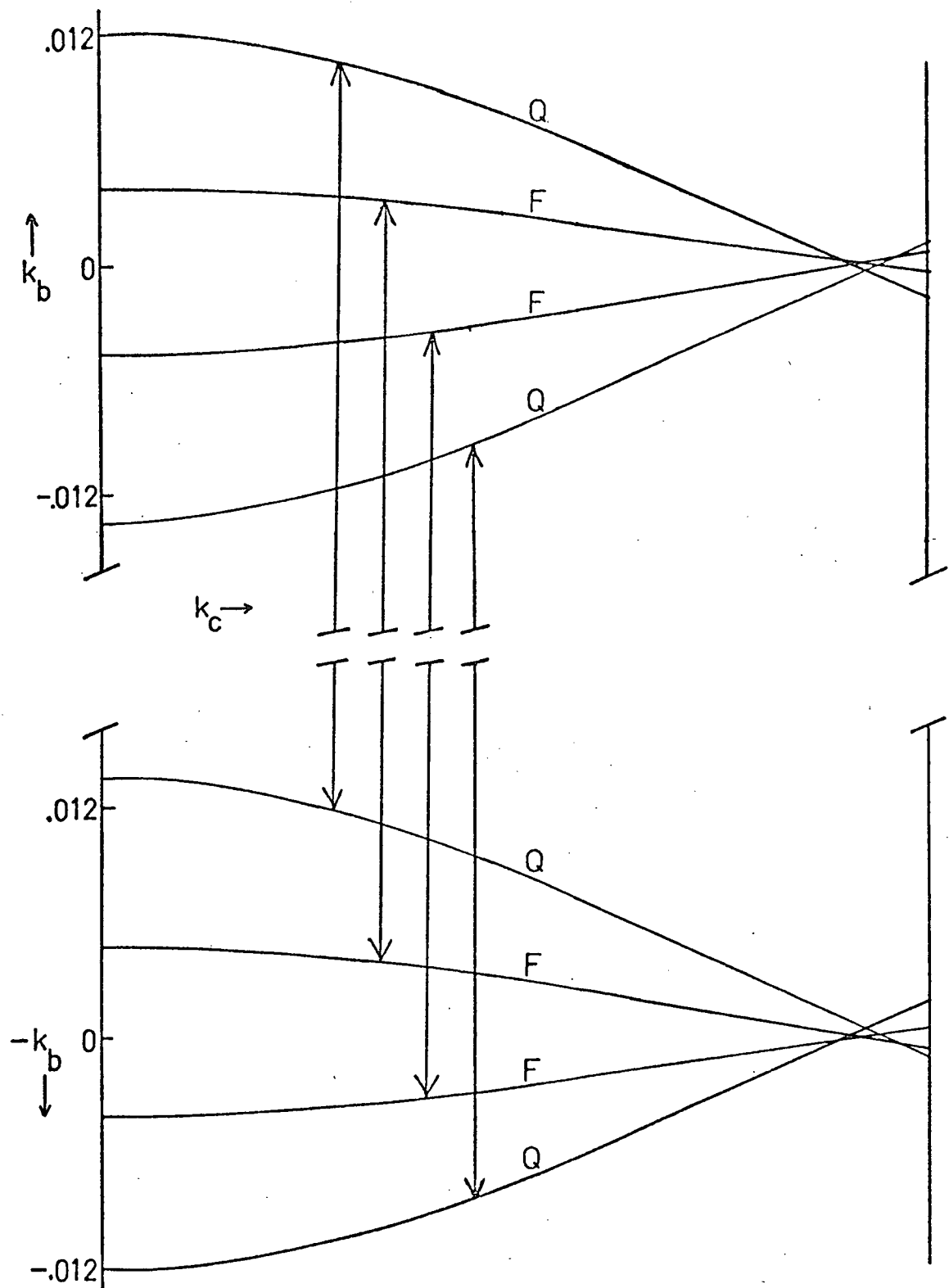Figure 7. Cross-section of the Fermi surface in the $\vec{b}$-$\vec{c}$ plane. The vertical scale represents the deviation (in units of π/b) of the surface from the planes $k_b = \pi/4b$ and $k_b = -\pi/4b$. Arrows show the nesting wavevectors.

Table 1. Molecular coordinates in TTF-TCNQ for those molecules shown in Fig. 3. In the coordinate system used, the lattice vectors are, in $\overset{\circ}{A}$ units: $\vec{a} = (12.298,0,0)$, $\vec{b} = (0,3.819,0)$, $\vec{c} = (-4.61,0,17.883)$.

	X	Y	Z
1	6.149	0	0
2	6.149	3.819	0
3	3.843	1.910	8.942
4	12.298	0	0
5	12.298	3.819	0
6	9.992	1.910	8.942

Table 2. Overlap integrals s_{ij}^m between MO's centered on the molecules listed in Table 1 and shown in Fig. 3 (taken from Berlinsky et al., 1974).

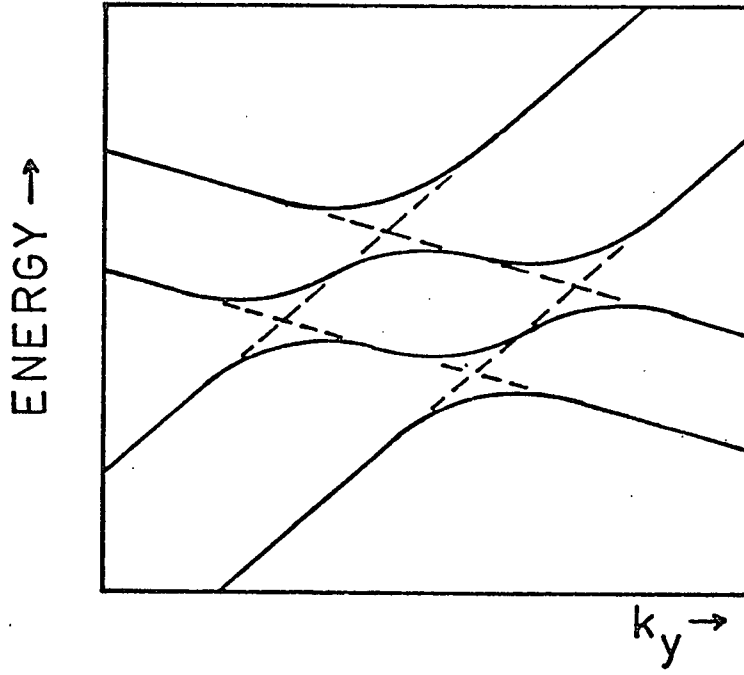|	1	2	3	4	5	6
1	1	2.0×10^{-2}	-3.0×10^{-4}	0	1.4×10^{-4}	1.8×10^{-7}
2	2.0×10^{-2}	1	-3.0×10^{-4}	-1.4×10^{-4}	0	3.3×10^{-4}
3	-3.0×10^{-4}	-3.0×10^{-4}	1	1.7×10^{-6}	3.4×10^{-4}	0
4	0	-1.4×10^{-4}	1.7×10^{-6}	1	-9.3×10^{-3}	4.8×10^{-5}
5	1.4×10^{-4}	0	3.4×10^{-4}	-9.3×10^{-3}	1	4.8×10^{-5}
6	1.8×10^{-7}	3.3×10^{-9}	0	4.8×10^{-5}	4.8×10^{-5}	1

Figure 8. Effect of the F-Q coupling on the bands in Fig. 6.

$$S_{32} = S_{23}^{*} = \sigma_{FQ}^{2}(e^{-i\vec{k}\cdot(\vec{b}+\vec{c})} - e^{i\vec{k}\cdot\vec{a}})$$

$$S_{41} = S_{14}^{*} = \sigma_{FQ}^{2}(e^{i\vec{k}\cdot(\vec{a}+\vec{c})} - e^{i\vec{k}\cdot\vec{b}})$$

$$H_{ij} = K(\epsilon_{F}^{o} + \epsilon_{Q}^{o})S_{ij}/2$$

(25)

The energy bands in various directions in the Brillouin Zone (Fig. 17) are shown in Fig. 9. The most striking frature of the bands is that they are very nearly flat, demonstrating the 1-D nature of TTF-TCNQ. A further corroboration of this observation is the appearance of the density of states which has been calculated for 5246 wavevectors in the Zone. The histogram plotted in Fig. 10 is nearly identical to the sketch in Fig. 5. The inset of Fig. 10 shows the density of states calculated for a finer mesh of wavevectors near the band crossing. The small peaks on either side of the dip arise from the mutual repulsion of the bands while the dip itself is due to the gap opened up in most directions.
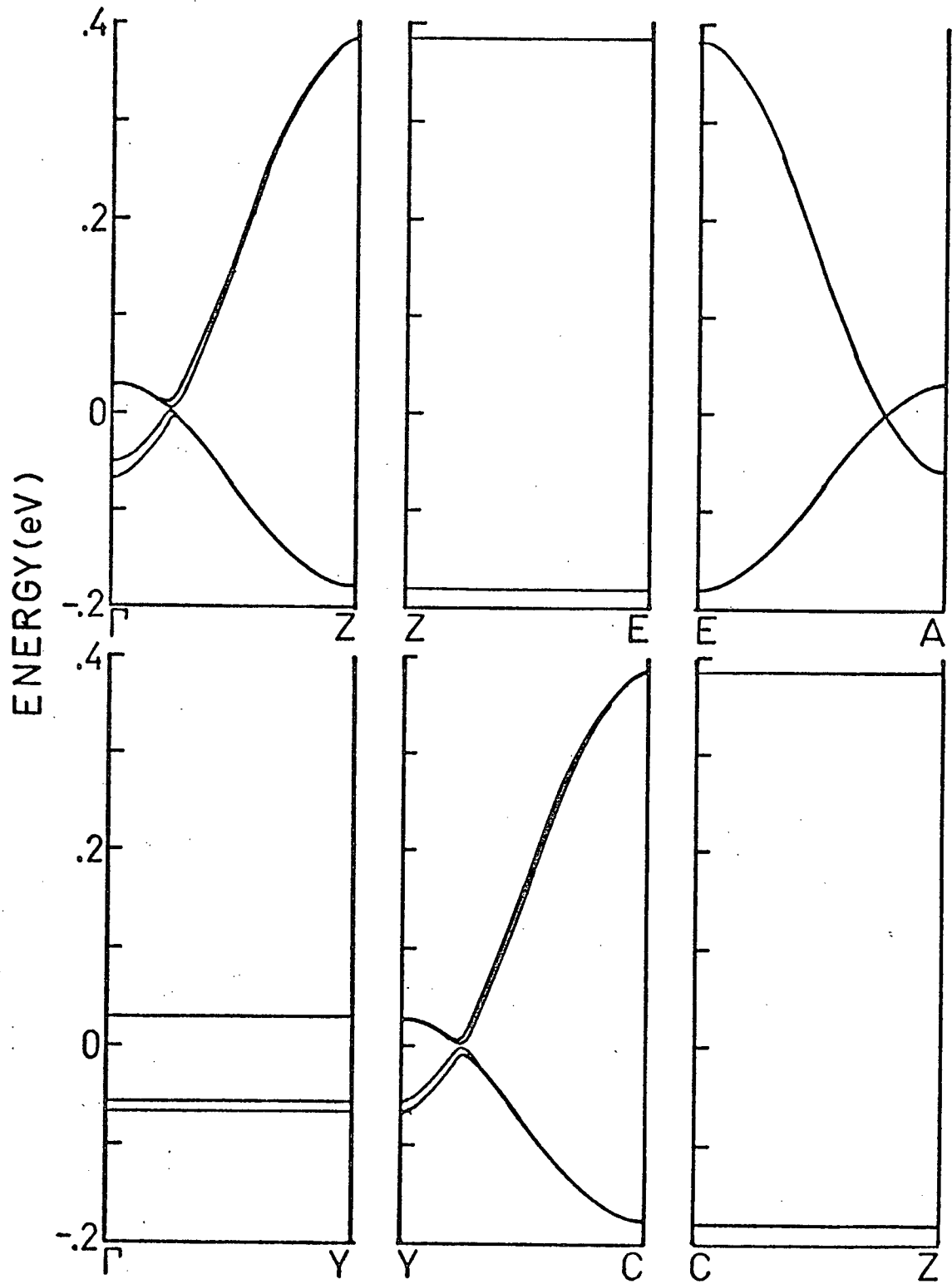
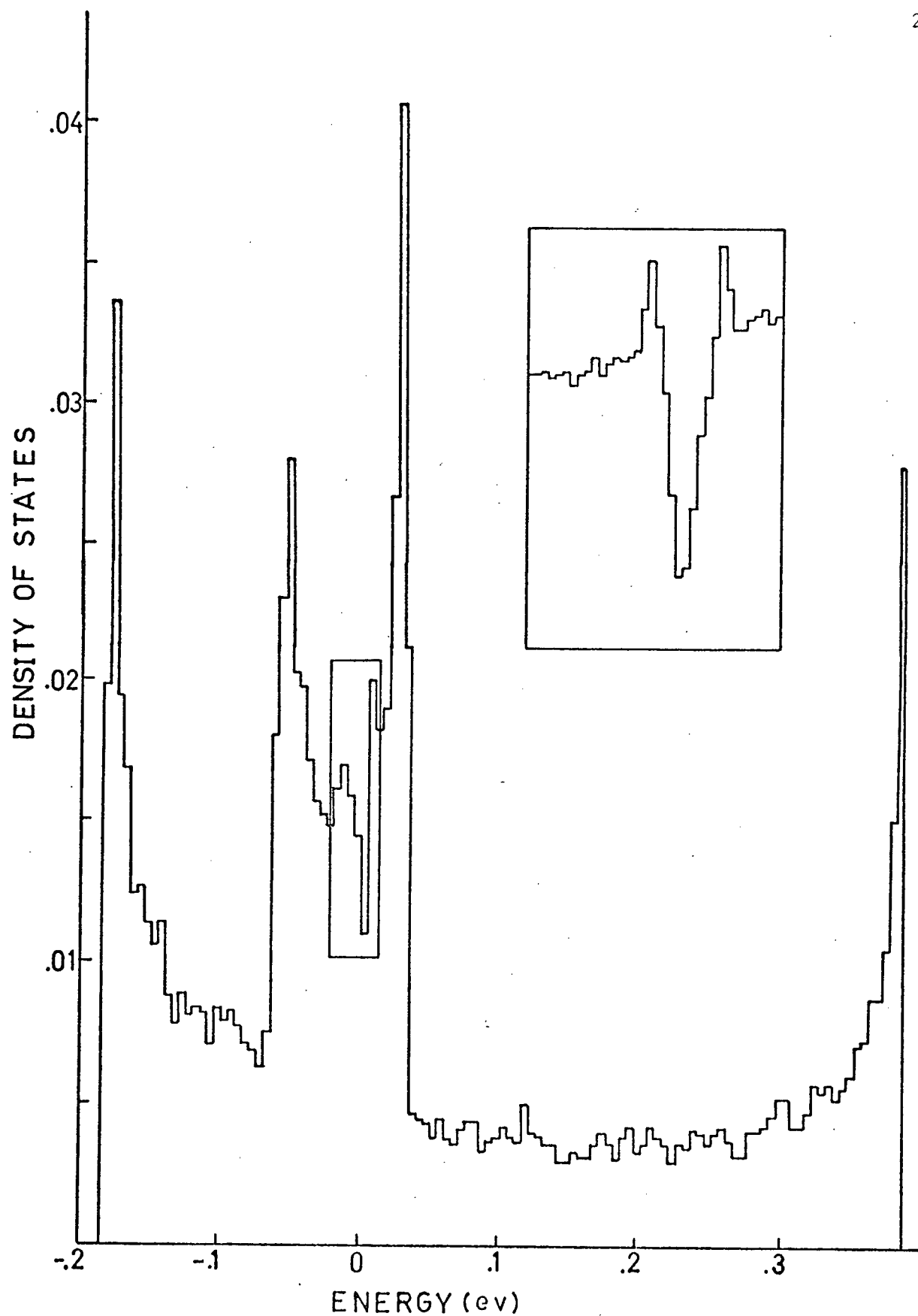Figure 9. Three-dimensional energy bands along several directions in the Brillouin Zone which is shown in Fig. 17.

Figure 10. Histogram of the density of states for the 3-D band structure. Inset: density of states near the Fermi level.
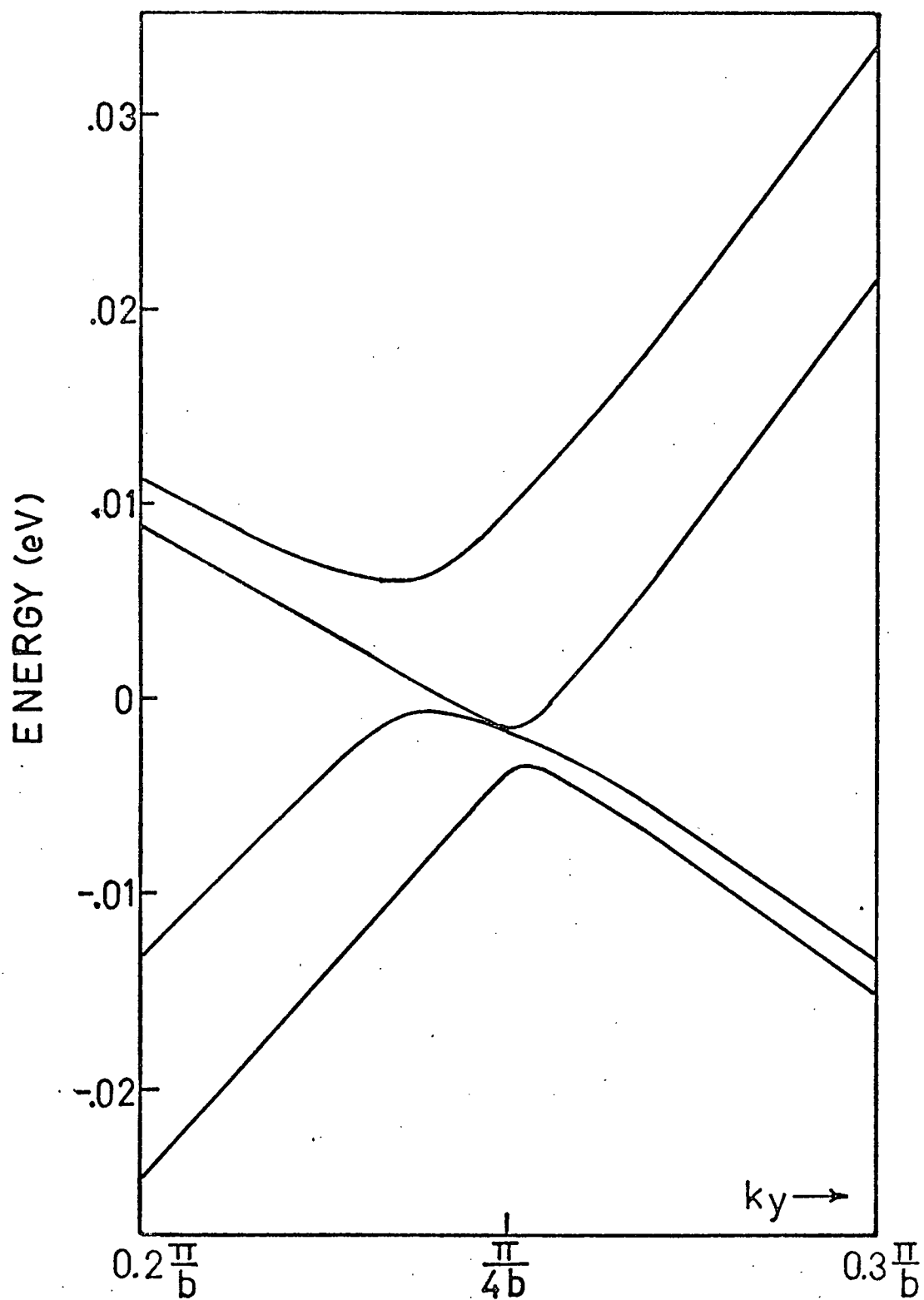
Figure 11. Energy bands near the Fermi energy in the ΓZ direction.

The crossover region along the ΓZ direction is shown in expanded scale in Fig. 11. To picture the Fermi surface it is convenient to view the bands throughout the Brillouin Zone as a large number of curves similar to the ones along ΓZ. Because of the flatness of the bands the top of the valence band, $\epsilon_v(k_a, k_c)$, and the bottom of the conduction band, $\epsilon_c(k_a, k_c)$, will deviate only slightly in energy through the Zone. Since the indirect overlap of the bands is very small, the Fermi level lies very close to ϵ_v and ϵ_c, intersecting both bands, only one band, or neither band, creating hole and electron surfaces. It must be pointed out that because the overlap of the bands is small the shape of the Fermi surface is quite sensitive to even small changes in the bands. In addition a precise determination of the Fermi energy is difficult and probably not meaningful, given the inaccuracies inherent in the method of calculation. Nevertheless, in order to gain a qualititive idea of the Fermi surface a Fermi energy was guessed ($E_F = -7.51$ eV) using the calculated band structure.

Cross-sections of the Fermi surface in several planes are shown in Fig. 12; as expected the surface consists of a very flat electron and hole pocket in each half of the Zone. While the value $E_F = -7.51$ eV is likely a little too low, a slightly higher energy would not make any qualitative difference, decreasing the size of the electron surface somewhat and increasing the hole surface. In any case, the extremely small degree of curvature in the surfaces makes it possible for different nesting vectors to connect various combinations of electron and hole surfaces. One of these possibilities is the wavevector with the component $q_b = \pi/2b$ linking a hole surface with an electron surface in the opposite half of the Zone. However, it is not apparent why the observed distortion is $(\pi/a, \pi/2b, \pi/nc)$.
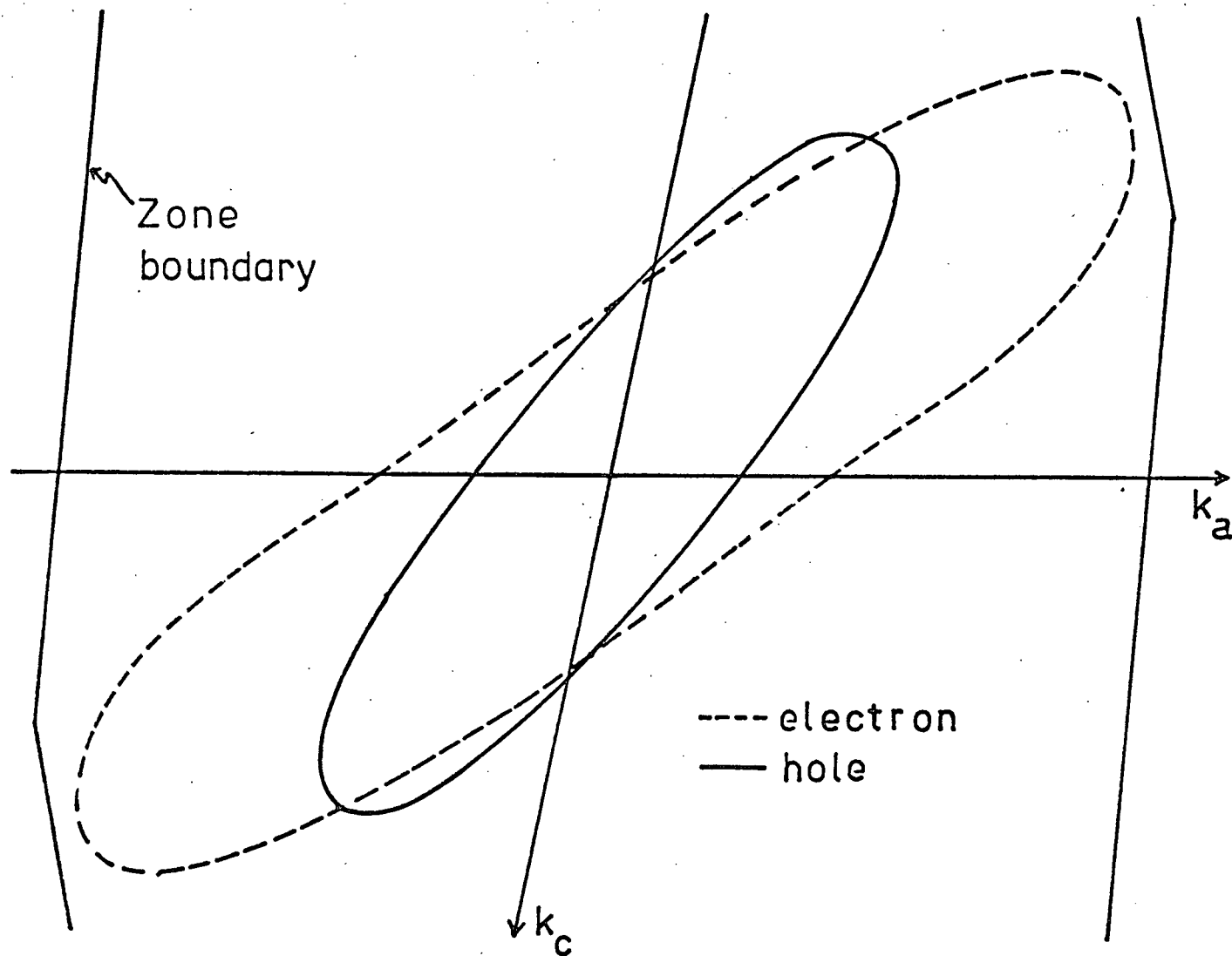
Figure 12. (a) Superimposed cross-sections of the electron and hole surfaces in two different planes parallel to $k_b = 0$.
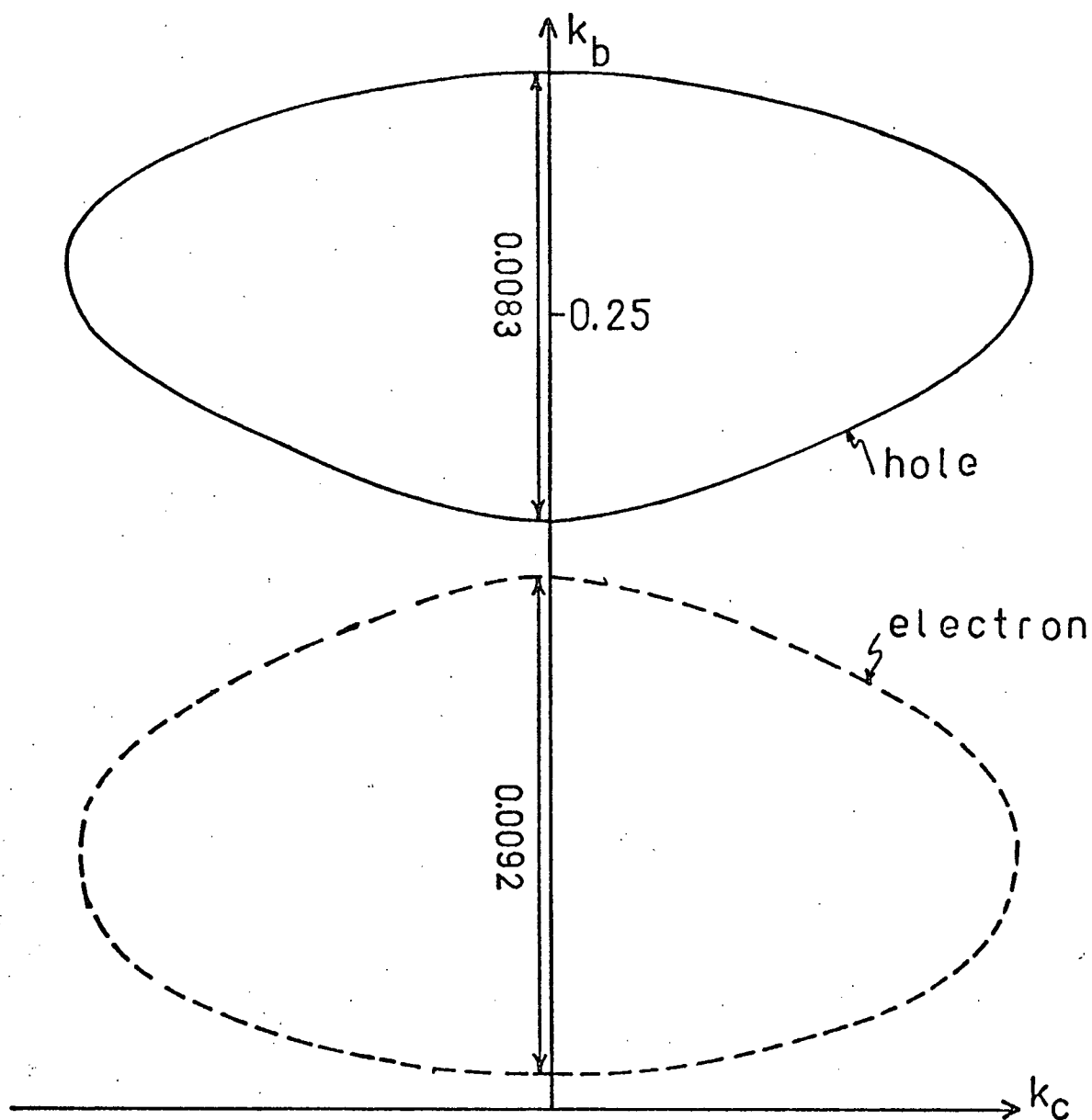
Figure 12. (b) Cross-section of the Fermi surface in the $k_a = 0$ plane. Shown are the electron and hole contours in the upper half of the zone. The vertical scale is in units of π/b

Chapter 3: (SN)x

3.1 Crystal Structure

Two determinations of the (SN)x crystal structure have recently be-
come available. The results of the first, an electron diffraction study
by Boudeulle (1974), are shown in Fig. 13 and are used in the calculations
presented in the remainder of the chapter. A later report by Cohen et al.
(1975) based on X-ray diffraction measurements gives a somewhat different
structure (see Appendix) in which the lattice constants are nearly the
same but the atomic bond angles are different from those of Boudeulle.

Calculations incorporating the Cohen data are presented in the Appen-
dix. Despite the difference in crystal structure the results are essen-
tially the same. Thus, the fact that the electron diffraction method is
less reliable is of little consequence in our study.

The crystal structure of (SN)x resembles that of TTF-TCNQ; in fact,
the space group $P2_1/c$ is the same. Sulphur and nitrogen atoms stack along
the b-axis forming alternating short (1.58 Å) and long (1.72 Å) SN bonds
such that four atoms per chain are included in the unit cell. Nearest-
neighbouring chains in the c-direction are related by inversion and are
thus inequivalent, giving a total of eight atoms per unit cell. The atomic
coordinates are listed in Table 3.

3.2 One-Dimensional Band Structure

As in the preceding discussion of TTF-TCNQ, we first consider the
case of isolated chains. The wavefunction $\Psi_k(r)$ is written as,
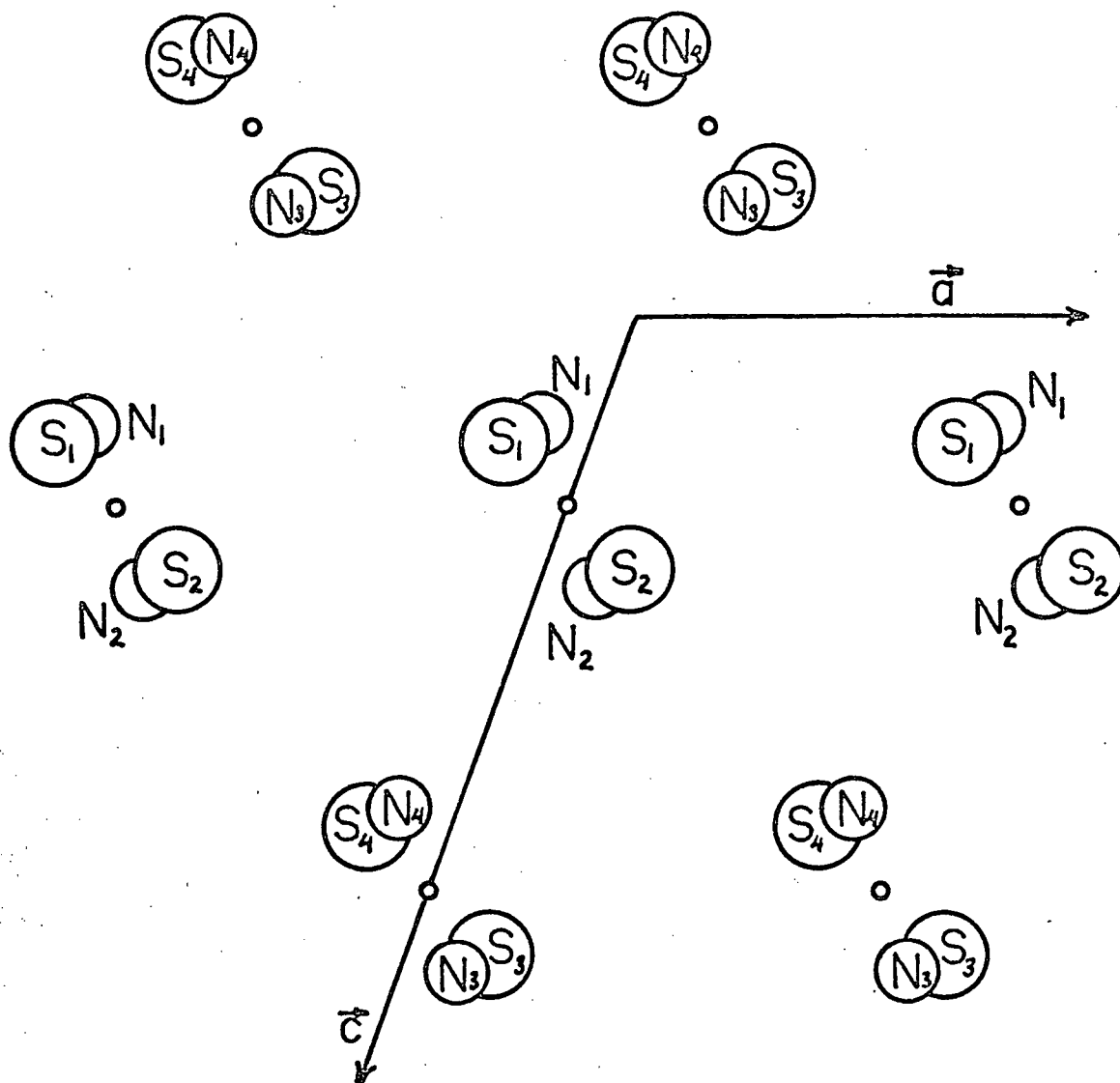
Figure 13. (a) Projection of the crystal structure of (SN)x onto a plane perpendicular to the chain axis. The sulphur and nitrogen atoms have been labelled S_i and N_i, i = 1,2,3,4 depending on the position in the unit cell.
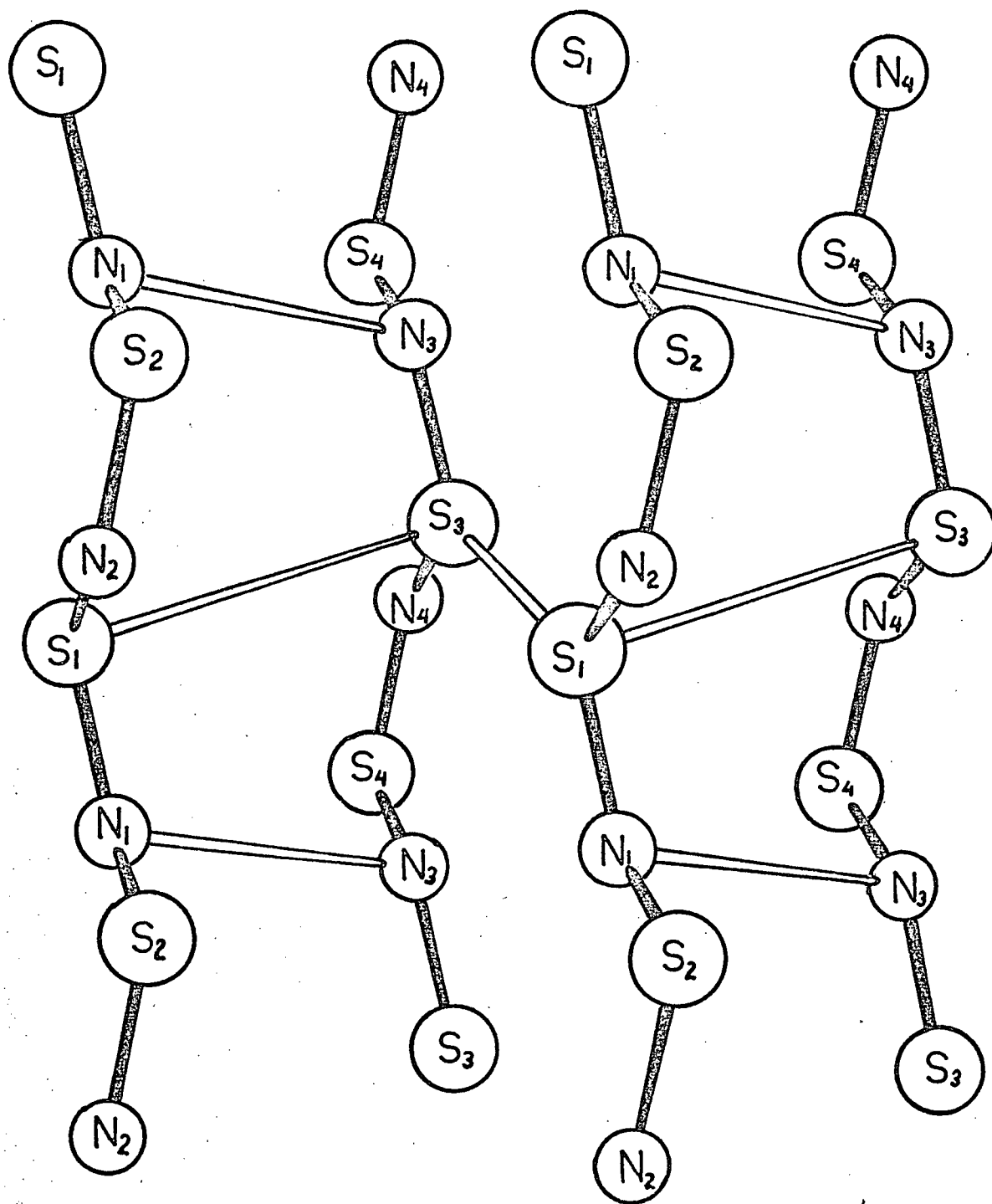
Figure 13. (b) Perspective drawing of a side view of the crystal struc-
ture. The solid rods indicate the bonds along the chain and
the open rods represent the most important interchain
overlaps discussed in §3.3.

Table 3. Atomic coordinates in the (SN)x unit cell for the Boudeulle structure. In the coordinate system used, the lattice vectors are, in Å units: $\vec{a}$ = (4.12,0,0), $\vec{b}$ = (0,4.43,0), and $\vec{c}$ = (-2.55,0,7.20). The b-axis is the chain axis.

	X	Y	Z
S_1	-1.20	1.74	1.20
S_2	-0.08	-0.48	2.40
S_3	1.20	-1.74	-1.20
S_4	0.08	0.48	-2.40
N_1	-0.90	0.20	1.05
N_2	-0.38	-2.02	2.55
N_3	0.90	-0.21	-1.05
N_4	0.38	2.02	-2.55

$$\Psi_{\vec{k}}(\vec{r}) = \frac{1}{\sqrt{N}} \sum_{j} \sum_{m} e^{i\vec{k} \cdot (\vec{R}_m + \vec{r}_j)} c_j^{\vec{k}} \psi_j(\vec{r}) \tag{26}$$

Here N is the number of unit cells, $\vec{R}_m$ is the coordinate of the center of the m'th cell, $\vec{r}_j$ is the coordinate with respect to the center of the cell of the j'th orbital, and $\psi_j(\vec{r})$ is an atomic Slater orbital. $\Psi_{\vec{k}}(\vec{r})$ was substituted into the Hückel formula using the constants ε_{2s} = -26.0, ε_{2p} = -13.4 eV, with Slater exponent 1.95 for nitrogen, and ε_{3s} = -20.0, ε_{3p} = -11.0 eV with Slater exponents 2.122 and 1.827 for sulphur.

Inclusion of the sulphur 3d orbitals in the basis set was found to result in a narrowing of the bands near the Fermi level with no other qualitative changes in the band structure. In some of the Hückel calculations mentioned in §1.5 the value K = 2.0 for the Wolfsberg-Helmholtz constant was found to lead to better results that the more popular value K = 1.75. An increased K produces broader bands, an effect opposite to the inclusion of the 3d states. Thus it was felt that we were safe in taking K = 1.75 and neglecting the 3d orbitals in our calculation.

Since the single chain unit cell consists of four atoms, $(SN)_2$, the energies for each k-value are obtained by solving a 16 x 16 eigenvalue equation. Fig. 14a shows the energy bands which result. Since the $(SN)_2$ unit has 22 valence electrons, the 11 lowest bands will be exactly filled at T = 0. Ordinarily one would then expect (SN)x to be an insulator. However, the screw axis symmetry of the crystal structure requires pairs of bands to be degenerate at the Zone boundary; since an odd number of bands are filled there is no gap at the Zone boundary. The density of states for the highest occupied and lowest unoccupied bands is shown in Fig. 15 (cf. Fig. 5).

(a)   (b)
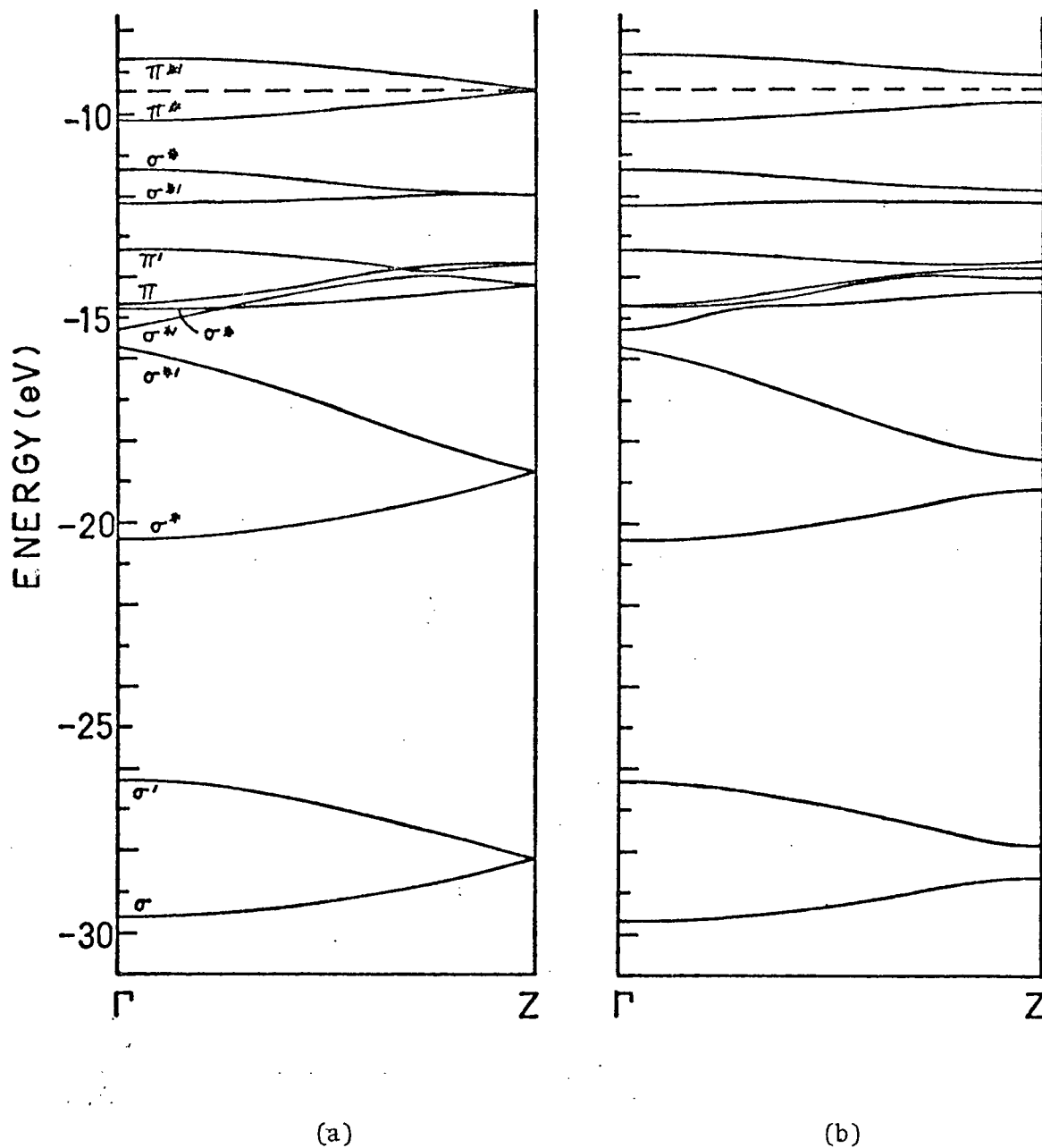
Figure 14. Energy bands for an isolated (SN)x chain. (a) For the observed
          structure. The symmetry labels are defined in the text while
          the dashed line represents the Fermi level. (b) For the
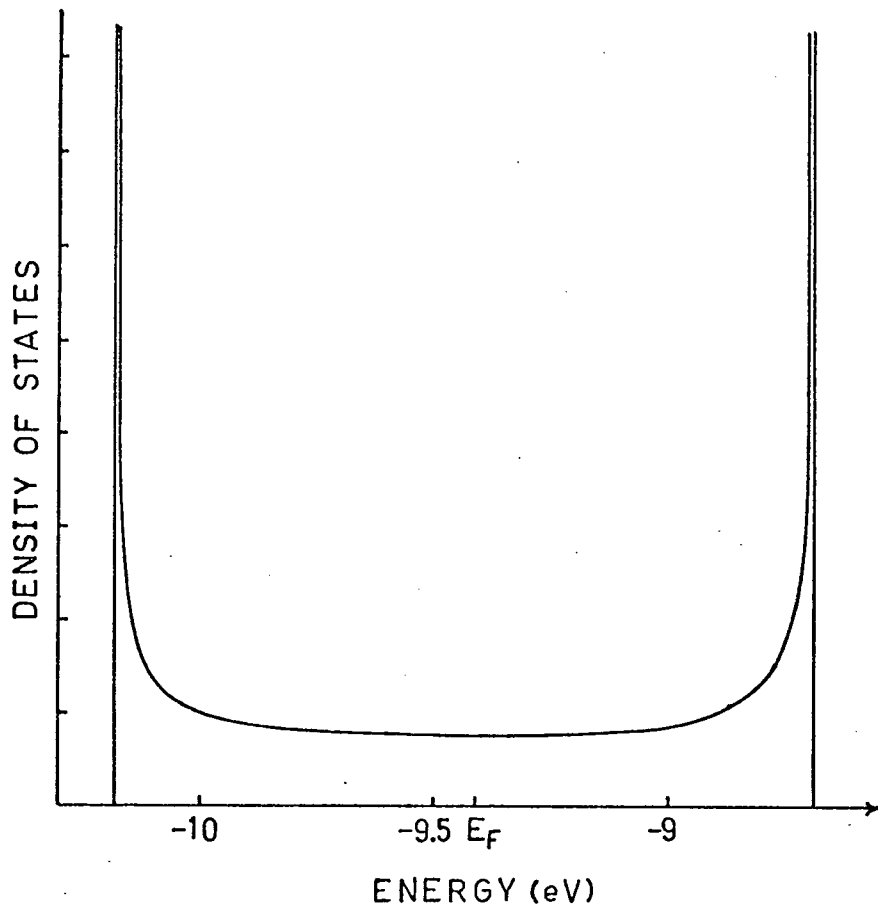   distorted structure shown in Fig. 16.

Figure 15. Density of states for the two bands straddling the Fermi
energy in Fig. 14a.

Because the chains are nearly planar, the labels σ or π may be used

to indicate orbitals which are approximately symmetric or anti-symmetric

upon reflection through this plane. The bands in which the k = 0 orbitals

have a node along the short SN bond are labelled by *, and ' labels a

k = 0 orbital with a node on the long SN bond. These results agree with

the calculation of Parry and Thomas (1975) who used a slightly different

version of the EHM.

It is obvious that since the degeneracy at the Zone boundary is due

to the screw axis symmetry, any distortion of the chain which breaks the

symmetry will open a gap at the Fermi level. One example of such a

distortion is illustrated in Fig. 16 (note that the size of the unit cell remains unchanged).
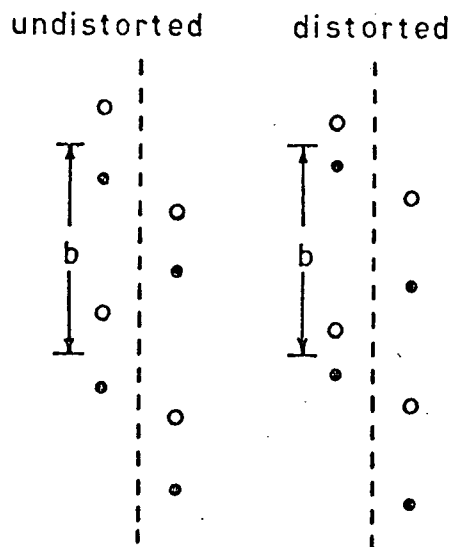

Figure 16. Distortion which breaks the screw axis symmetry.

The effect of such a distortion in which the short bondlength is changed by 0.1 $\overset{\text{o}}{\text{A}}$ is demonstrated in Fig. 14b. We conclude, therefore, that because of this instability (SN)x should be a semiconductor.

3.3 Three-Dimensional Band Structure

Boudeulle has pointed out that some of the S-S and N-N distances between atoms on different chains are less than twice the Van der Waals radii for sulphur and nitrogen. The interchain coupling should then be relatively large, implying that the 1-D approximation is not very good. Since there are two chains per unit cell, the 1-D bands are doubly degenerate, the degeneracy being removed by the interchain coupling. The splitting of the bands shifts the Fermi level away from the Zone boundary, while

hybridization between the bands causes a splitting were the bands should cross.

A full 3-D band structure taking into account an $(SN)_2$ unit on one chain in a unit cell with 20 neighbouring $(SN)_2$ units (two on the same chain and three on each of six surrounding chains) has been calculated and is shown along several symmetry directions of the Brillouin Zone (Fig. 17) in Fig. 18. The lines and planes of degeneracies which arise are the result of the screw axis and time reversal symmetry. The important feature in Fig. 18 is the crossing of the bands in ΓZ and YC directions while there are gaps in all the other directions. The crossings are accidental degeneracies and are allowed because the wavefunctions of the crossing bands transform differently under the screw axis symmetry operation.

An accurate determination of the Fermi level is not easily obtained. Qualitatively, however, it is not difficult to visualize the appearance of the Fermi surface. The crossings along ΓZ and YC occur at different energies so that the Fermi level intersects the bands at points other than the degenerate points. One thus expects a Fermi surface consisting of an electron pocket near the crossing along YC and a hole pocket near the crossing on ΓZ, leading us to describe (SN)x as a semimetal.

It is gratifying to note that our results agree qualitatively with the more sophisticated relativistic OPW calculations of Rudge (1975). The most important feature of Rudge's that is not present in our results is the lower band in the ZE direction rising across the Fermi level, creating a hole pocket near point E. His conclusion reinforces ours that (SN)x is a semimetal.

The 3-D band structure is obtained from a 32 x 32 eigenvalue equation that is cumbersome to work with. A simplified treatment can be made by
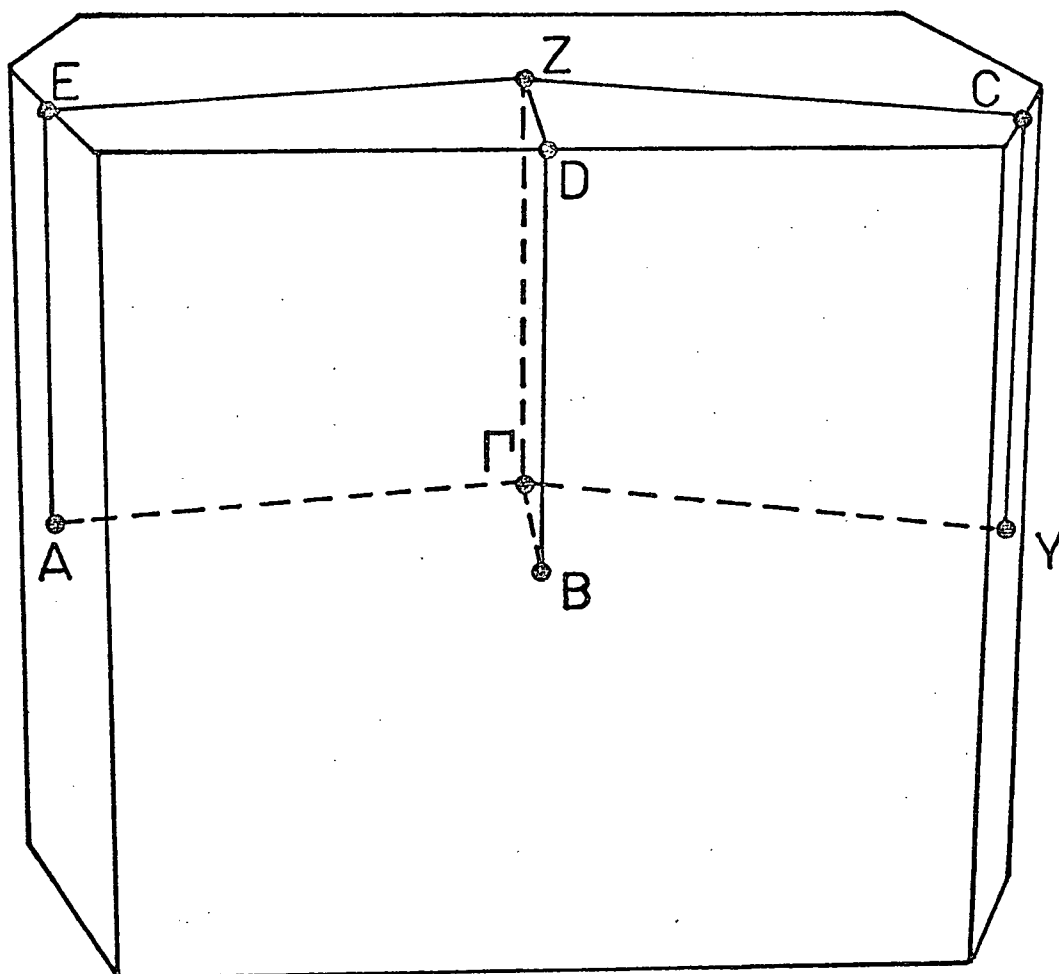
Figure 17. Brillouin zone associated with the crystal structures of (SN)x and TTF-TCNQ. Symmetry dictates two-fold degeneracies in the band structure throughout the top and bottom zone faces and along the lines AE and BD. CY is not a line of degeneracy.

Figure 18. Three-dimensional band structure in those directions indicated in Fig. 17 as obtained from the extended Hückel calculation. Only the four bands closest to the Fermi level are shown. The dashed line marks the approximate position of the Fermi energy.

noting that the highest occupied and lowest unoccupied bands in the 1-D

calculation (Fig. 14a) look very much like simple tight-binding (cosine)

bands. The k = 0 wavefunction symmetries indicated in Fig. 14a suggest
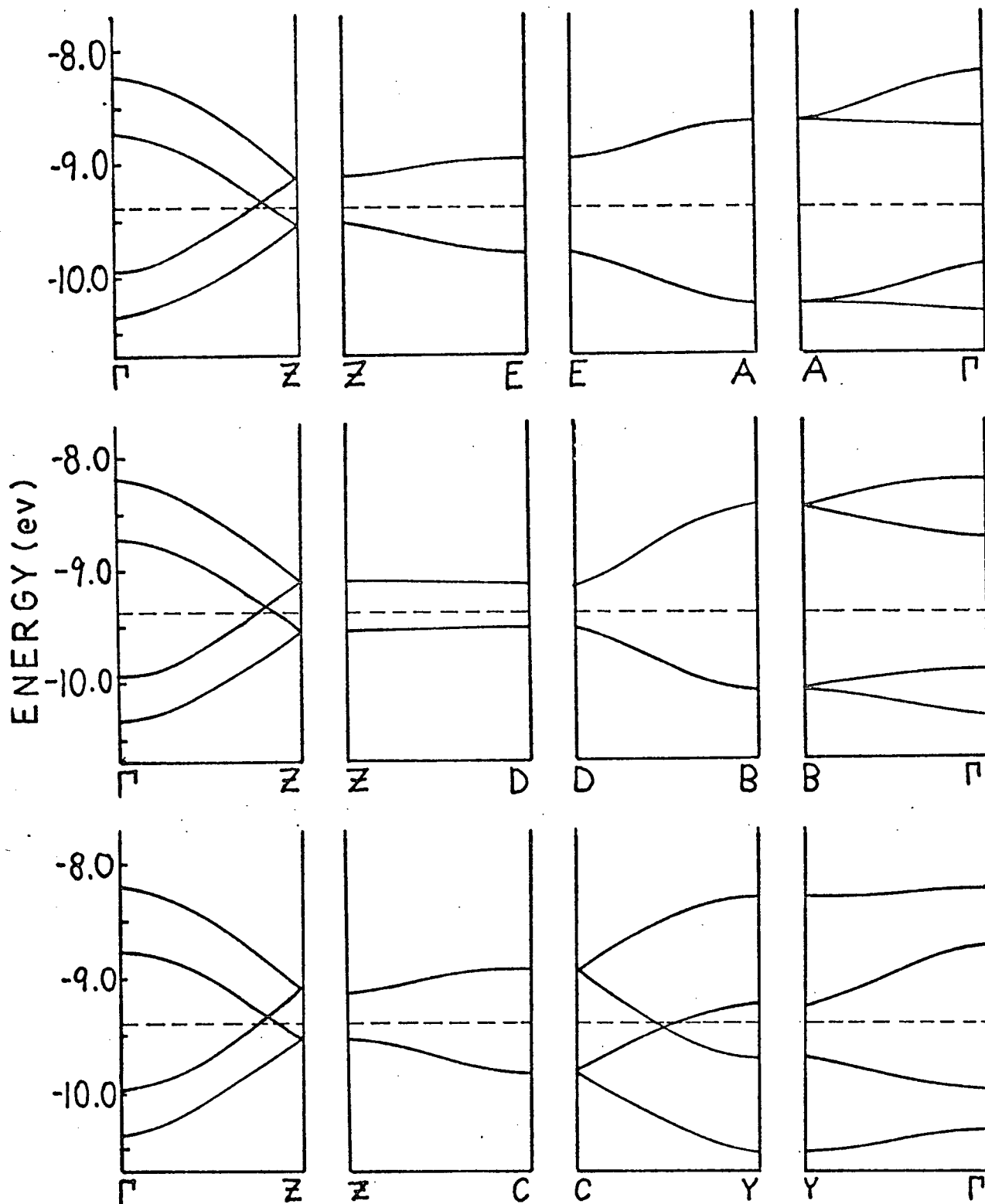
that a suitable basis for such a calculation might be a π^* SN molecular

orbital. There are four such SN molecules per unit cell leading us to

consider a 4 x 4 model Hamiltonian. An important simplification of the

matrix can be obtained by a closer examination of the crystal structure

(Table 2 and Fig. 13). The molecule labelled S_1N_1 is considerably farther

away from molecules labelled S_4N_4 in its own and in neighbouring cells

than from those labelled S_2N_2 and S_3N_3. Taking symmetry into account, it

should be a good approximation to neglect matrix elements along the anti-

diagonal; the validity of this approximation is confirmed by a calculation

of the overlaps. The Hamiltonian then takes the form (if the energy of

the SN MO is taken to be 0),

$$H \quad = \quad \begin{bmatrix} 0 & \mu^* & \delta_1^* & 0 \\ \mu & 0 & 0 & \delta_2^* \\ \delta_1 & 0 & 0 & \mu \\ 0 & \delta_2 & \mu^* & 0 \end{bmatrix} \tag{27}$$

Expansion of the corresponding secular determinant gives a characteristic

equation of the form,

$$\epsilon^4 - 2\alpha\epsilon^2 + \beta = 0 \tag{28}$$

with roots,

$$\epsilon = \pm\sqrt{\alpha \pm \sqrt{\alpha^2 - \beta}} \tag{29}$$

where,

$$2\alpha = 2|\mu|^2 + |\delta_1|^2 + |\delta_2|^2$$

$$\beta = |\delta_1|^2|\delta_2|^2 + |\mu|^4 - \mu^2\delta_1\delta_2^* - \mu^{*2}\delta_1^*\delta_2$$

Quantitative results for this model can be obtained by examination of the wavefunctions coming out of the band structure calculation. The π^* SN MO which is suggested has the form,

$$\psi = \phi_S - \tfrac{1}{2}\phi_N \qquad (30)$$

The most important interactions involving these MO's are then:

    (i) t: the π-interaction between nearest-neighbouring molecules on the same chain.

    (ii) t_1: a π-interaction with a bond length of 3.10 $\overset{o}{A}$ between an atom S_1 and the atom S_3 in the cell displaced by $(\vec{b} - \vec{a})$.

    (iii) t_2: a σ-interaction with bond length 2.81 $\overset{o}{A}$ between atoms N_1 and N_3 in the same unit cell.

    (iv) t_3: a σ-interaction between S_1 and S_3 in the cell displaced by $\vec{b}$.

Including symmetry-equivalent interactions gives for the matrix elements the expressions,

$$\mu = t(1 + e^{-i\vec{k}\cdot\vec{b}})$$
$$\delta_1 = t_1 e^{i\vec{k}\cdot(\vec{a}-\vec{b})} + t_2 + t_3 e^{-i\vec{k}\cdot\vec{b}}$$
$$\delta_2 = t_1 e^{-i\vec{k}\cdot(\vec{a}+\vec{c})} + t_2 e^{i\vec{k}\cdot(\vec{b}-\vec{c})} + t_3 e^{-i\vec{k}\cdot\vec{c}} \qquad (31)$$

The parameters t, t_1, t_2, t_3 can be calculated using the Hückel formula (13) and the SN MO. One then finds that t = 0.45 eV, t_1 = -0.22 eV,

t_2 = -0.06 eV, and t_3 = 0.56 eV. Since these are only approximate values, we have chosen a set of parameters (t = 0.45 eV, t_1 = -0.19 eV, t_2 = -0.05 eV, and t_3 = 0.42 eV) which better reproduce the band structure of Fig. 18; these tight-binding curves are presented in Fig. 19.

Two important features of the band structure are readily apparent from equation (29):

(i) When $\alpha^2 = \beta$, $\varepsilon = \pm\sqrt{\alpha}$ and the band structure exhibits a two-fold degeneracy. The directions in $\vec{k}$-space for which this occurs are exactly those for which symmetry dictates degeneracies.

(ii) An accidental degeneracy occurs when β = 0. Then ε = 0 and the bands cross at the Fermi level. β = 0 when

$$\mu^2 = \delta_1 \delta_2^*$$ (32)

Taking the real and imaginary parts of the equation gives two equations, the solution of which defines a curve in $\vec{k}$-space, which, with the parameters chosen extends from $(0, 0.8\pi/b, 0)$ to $(\pi/a, 0.5\pi/b. 0.33\pi/a)$. The simple form of the energy bands described by (29) means that all band crossings occur at the Fermi level. The conclusion of this oversimplified model therefore is that (SN)x is a zero-gap semiconductor.

A sophistication of this model to include non-zero terms along the anti-diagonal and interactions with other bands would remove the accidental degeneracy at tht Fermi level. One would expect the small splittings to cause indirect overlaps of the bands, thereby creating a Fermi surface of a semimetal with electron and hole pockets. This conclusion agrees with that of the more complex Hückel calculation.

Since a density of states calculation incorporating the full Hückel treatment proved to be unfeasible, the tight-binding bands were used as
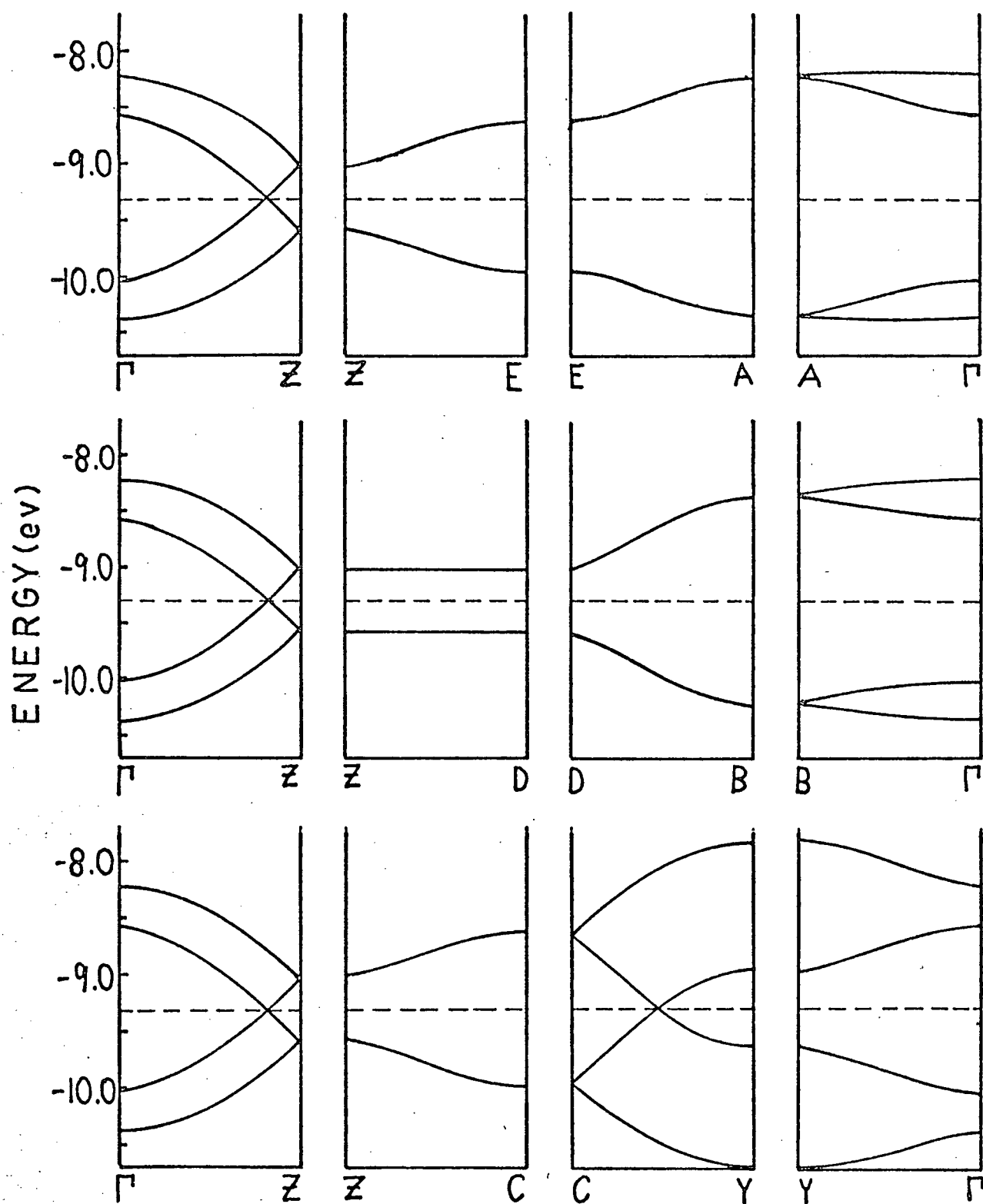
Figure 19. Band structure analogous to that of Fig. 18 resulting from
the tight-binding calculation.

they represent the energy bands reasonably well. Fig. 20 shows the results, and while the details of the plot are not believable, the overall features should be correct. The lack of resemblance to the 1-D density of states in Fig. 15 is an indication of the dispersion of the bands in directions transverse to the chain axis and clearly demonstrates the need for a 3-D model of (SN)x.

Other authors who have calculated the band structure and the methods they have used are:

(i) Rajan and Falicov (1975), ab initio.

(ii) Kamimura et al. (1975), semi-empirical.

(iii) Schlüter et al. (1975), pseudopotential.

The feature these calculations have in common is a Fermi level which intersects overlapping σ and π bands, differing in this regard from our results. A possible explanation of the situation (Weiler) is that these methods overestimate the splitting of low-lying σ bands in the solid, pushing them up in energy and causing them to mix with the π bands. The use of the EHM for (SN)x thus seems to be partly justified.
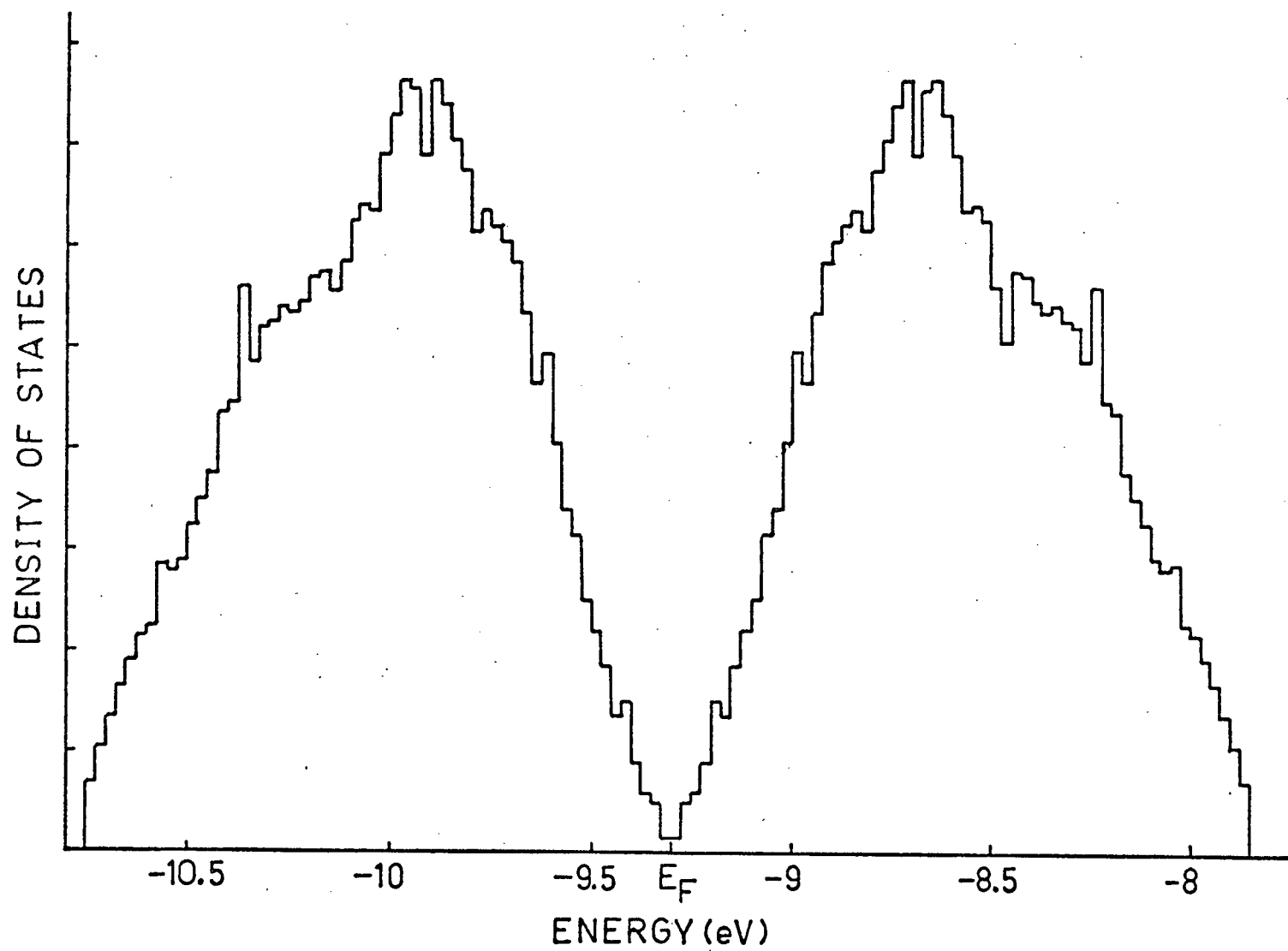
Figure 20. Density of states for the 3-D tight-binding calculation.

Chapter 4: Discussion

In the preceding two chapters we have considered the electronic energy spectra of two outwardly similar systems. What we can conclude is that both TTF-TCNQ are semimetals, in agreement with experiment. Both materials also exhibit similar anisotropy in electrical conductivity and optical properties. Why then is it that TTF-TCNQ undergoes a Peierls transition to a semiconducting state while (SN)x not only does not show this feature but actually becomes superconducting?

To underscore the similarity let us take a closer look at the (SN)x crystal structure in the framework of our calculation. If one believes the simple tight-binding MO treatment, then a single (SN)x chain (type-I) can be looked upon as consisting of two inequivalent (type-II) chains, each contributing one SN "molecule" to the unit cell. The two "molecules", although structurally identical, might be labelled F and Q since they give rise to separate bands (the two with the degeneracy at the Fermi level in Fig. 14a). Regarding the second type-II chain in the same manner, one has two F and Q "molecules" per unit cell. In the 1-D approximation of §3.2, the two bands are doubly degenerate. Thus, in this picture, the (SN)x model is completely analogous to TTF-TCNQ except for differences in the intermolecular distances.

The difference between the two solids is immediately apparent when the interchain interactions are turned on. The effect is seen dramatically in the magnitude of the splittings of the degenerate bands. In (SN)x, the ratio of the splitting to the 1-D bandwidth is about 0.3 as compared to

a ratio of < 0.03 in TTF-TCNQ. Further, bandwidths (in terms of the band-width along ΓZ) in directions transverse to ΓZ range up to 0.1 for (SN)x, but are less than 0.01 for TTF-TCNQ. It seems, therefore, that the sup-pression of the Peierls transition in (SN)x must be attributed to the strong interchain coupling.

HGW explain the occurrence of a Peierls transition in TTF-TCNQ in terms of their results (see §1.4). From specific heat and electrical con-ductivity data they obtain a value of the interchain coupling $\eta \simeq 0.1$, which falls into the region given by (8) in which a 1-D mean field theory approach to the Peierls transition is valid. Whether or not this explana-tion is correct is not clear since our MO calculation gives a maximum $\eta = 0.015$ for two neighbouring TCNQ chains. Further, the HGW model fails to describe TTF-TCNQ as a two-component system with crossing bands inter-acting at the Fermi level to create a Fermi surface which differs from the one resulting from equations (6) and (7). However, the actual shape of the surface is likely not very important at temperatures near the ob-served $T_c \simeq 60K$, in light of the small dispersion of the energy bands transverse to the chain direction. Thus our calculation does not preclude the Peierls instability with wavevector $\vec{q} = (\pi/a, 2p_F, \pi/c)$ which HGW con-clude is favoured to occur.

As the band structure in Fig. 9 shows, TTF-TCNQ is well explained by a 1-D model and consequently the observed anisotropies in the electronic properties are not surprising. Similar observations for (SN)x which initially led to its being classified as a quasi-1-D material are inconsistent with the band structure in which 3-D effects are important. One must conclude, therefore, that the observed anisotropy is due in most part to the fibrous nature of the crystal.

Bibliography

Bardeen, J. 1973. Solid State Comm. 13, 357.

Berlinsky, A.J., Carolan, J.F., and Weiler, L. 1974. Solid State
    Comm. 15, 795.

Boudeulle, M. 1974. Thesis, Université de Lyon.

Chaikin, P.M., Kwak, J.F., Jones, T.E., Garito, A.F., and Heeger, A.J.
    1973. Phys. Rev. Lett. 31, 601.

Coleman, L.B., Cohen, M.J., Sandman, D.J., Yamagishi, F.G., Garito, A.F.,
    and Heeger, A.J. 1973. Solid State Comm. 12, 1125.

Cohen, M.J., Garito, A.F., Heeger, A.J., MacDiarmid, A.G., and
    Saran, M. 1975. To be published.

Craven, R.A., Salamon, M.B., DePasquali, G., Herman, R.M., Stucky, G.,
    and Schwertz, A. 1974. Phys. Rev. Lett. 32, 769.

Denoyer, F., Comès, R., Garito, A.F., and Heeger, A.J. 1975. Phys.
    Rev. Lett. 35, 445.

Etemad, S., Penney, T., Engler, E.M., Scott, B.A., and Seiden, E. 1975.
    Phys. Rev Lett. 34, 741.

Fleming, J.E., and Falk, R.J. 1973. J. Phys. C 6, 2954.

Fröhlich, H. 1954. Proc. Roy. Soc. A223, 296.

Goehring, M. 1956. Q. Rev. Chem. Soc. 10, 437.

Greene, R.L., Street, G.B., and Suter, L.J. 1975. Phys. Rev. Lett. 34, 577.

Grobman, W.D., Pollak, R.A., Eastman, D.E., Maas, E.T., Jr., and Scott, B.A.
    1974. Phys. Rev. Lett. 32, 534.

Hoffman, R. 1963. J. Chem. Phys. 39, 1397.

Horovitz, B., Gutfreund, H., and Weger, M. 1975. To be published.

Hsu, C., and Labes, M.M. 1974. J. Chem. Phys. 61, 4640.

Kamimura, H., Grant, A.J., Levy, F., and Yoffe, A.D. 1975. Solid State
    Comm. 17, 49.

Kistenmacher, T.J., Phillips, T.E., and Cowan, D.O. 1974. Acta Cryst.
    B30, 763.

Kohn, W. 1959. Phys. Rev. Lett. $\underline{2}$, 393.

Kortela, E.K., and Manne, R. 1974. J.Phys C 7, 1749.

Landau, L.D., and Lifschitz, E.M. 1969. $\underline{\text{Statistical Physics}}$ §152, (Addison-Wesley, Don Mills, Ontario).

Lee, P.A., Rice, T.M., and Anderson, P.W. 1973. Phys. Rev. Lett. $\underline{31}$, 462.

Little, W.A. 1964. Phys. Rev. A $\underline{134}$, 1416.

McCubbin, W.L., and Manne, R. 1968. Chem. Phys. Lett. $\underline{2}$, 230.

Parry, D.E., and Thomas, J.M. 1975. J. Phys. C $\underline{8}$, L45.

Peierls, R.E. 1955. $\underline{\text{Quantum Theory of Solids}}$ (Oxford University Press, London).

Rajan, V.T., and Falicov, L.M. 1975. To be published.

Rice, M.J., and Strässler, S. 1973. Solid State Comm. $\underline{13}$, 125.

Rudge, W. 1975. Bull. Am. Phys. Soc. $\underline{20}$, 359, and private communication.

Salamon, M.B., Bray, J.W., DePasquali, G., and Craven, R.A. 1975. Phys. Rev. B $\underline{11}$, 619.

Schafer, D.E., Wudl, F., Thomas, G.A., Ferraris, J.P., and Cowan, D.O. 1974. Solid State Comm. $\underline{14}$, 342.

Schlüter, M., Chelikowsky, J.R., and Cohen, M.L. 1975. To be published.

Tiedje, T., Carolan, J.F., Berlinsky, A.J., and Weiler, L. 1975. Can. J. Phys. $\underline{53}$ (to be published).

Tiedje, T. 1975. M.Sc. Thesis, University of British Columbia.

Tomkiewicz, Y., Scott, B.A., Tao, L.J., and Title, R.S. 1974. Phys. Rev. Lett. $\underline{32}$, 1363.

Weiler, L. Private Communication.

Appendix: (SN)x Band Structure for the Penn Crystal Structure

The structure of (SN)x reported by Cohen et al. (1975) of the University of Pennsylvania group differs from that of Boudeulle in two ways (although the lattice parameters are virtually identical). Firstly, the intrachain bonding angles are different, resulting in S-N bond distances which are almost equal (1.59 and 1.63 Å as compared to Boudeulle's 1.58 and 1.72 Å) and in chains which are very nearly planar as shown in Fig. A1. Secondly, inequivalent chains are translated with respect to each other by about 1 Å along the b-axis as compared to those in the Boudeulle structure. Table A1 lists the coordinates of the atoms in the unit cell.

The calculations of Chapter 3 have been repeated using the Penn data. Fig A2 shows the 3-D band structure arising from the full Hückel calculation. Overall, the bands resemble those of Fig. 18; the differences in detail which are evident are an increased bandwidth along ΓZ and a smaller band splitting which pushes the Fermi wavevector back out to the zone boundary. The implication, therefore, is that in the Penn structure the intrachain coupling is greater than in the Boudeulle structure while the interchain coupling decreases.

The tight-binding approximation to the band structure introduced in §3.3 has also been applied in this case. Because of the change in the relative position of the inequivalent chains, different interactions become important and the greatly simplifying feature that elements on the anti-diagonal are zero does not appear. Thus no expression such as (28) can be written down and the 4 x 4 Hamiltonian must be diagonalized numerically.

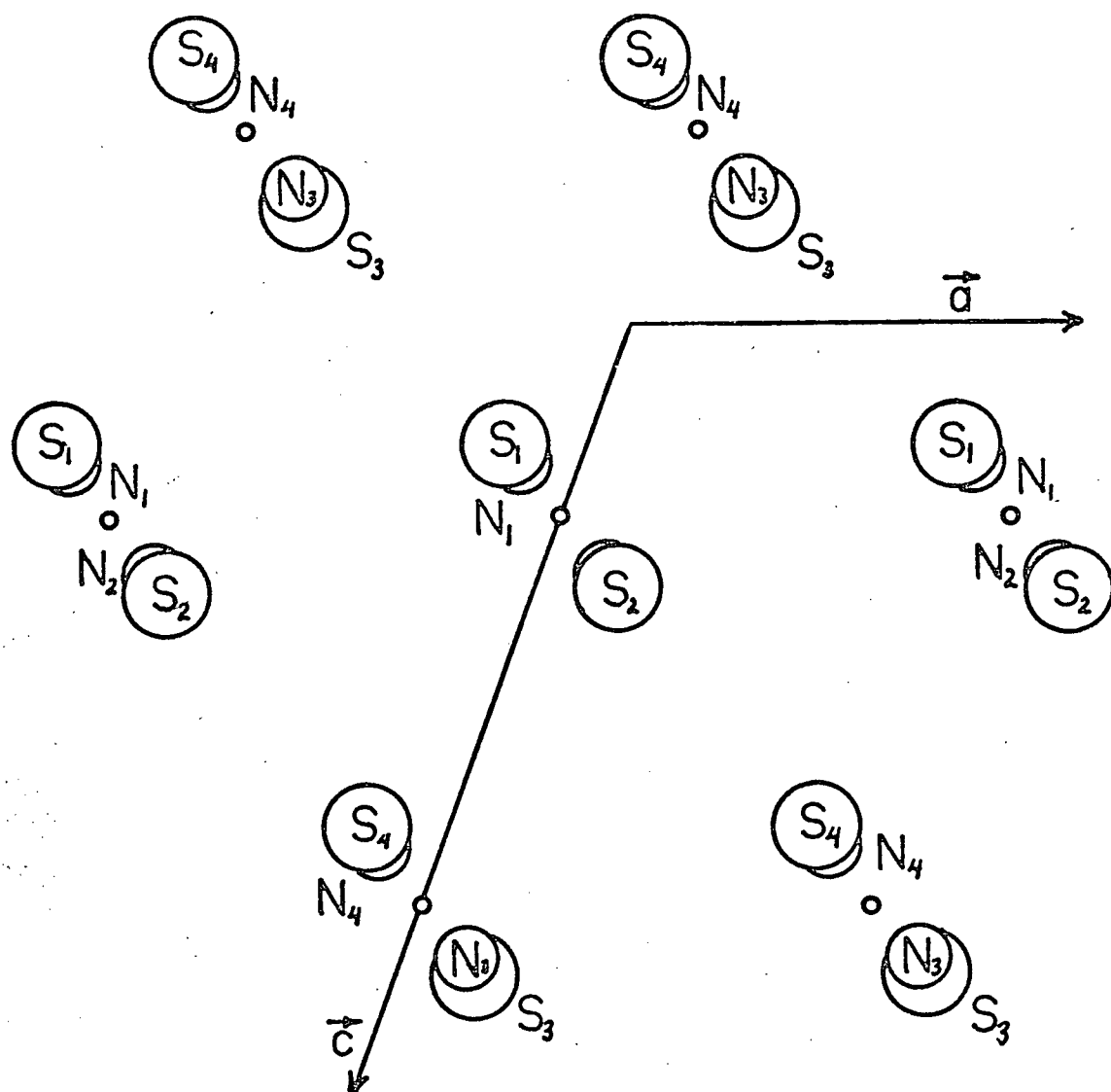If the energy of the SN MO's is taken to be zero, then the Hamiltonian

Figure A1. View down the b-axis of the crystal structure of (SN)x from the data of Cohen et al. (1975).
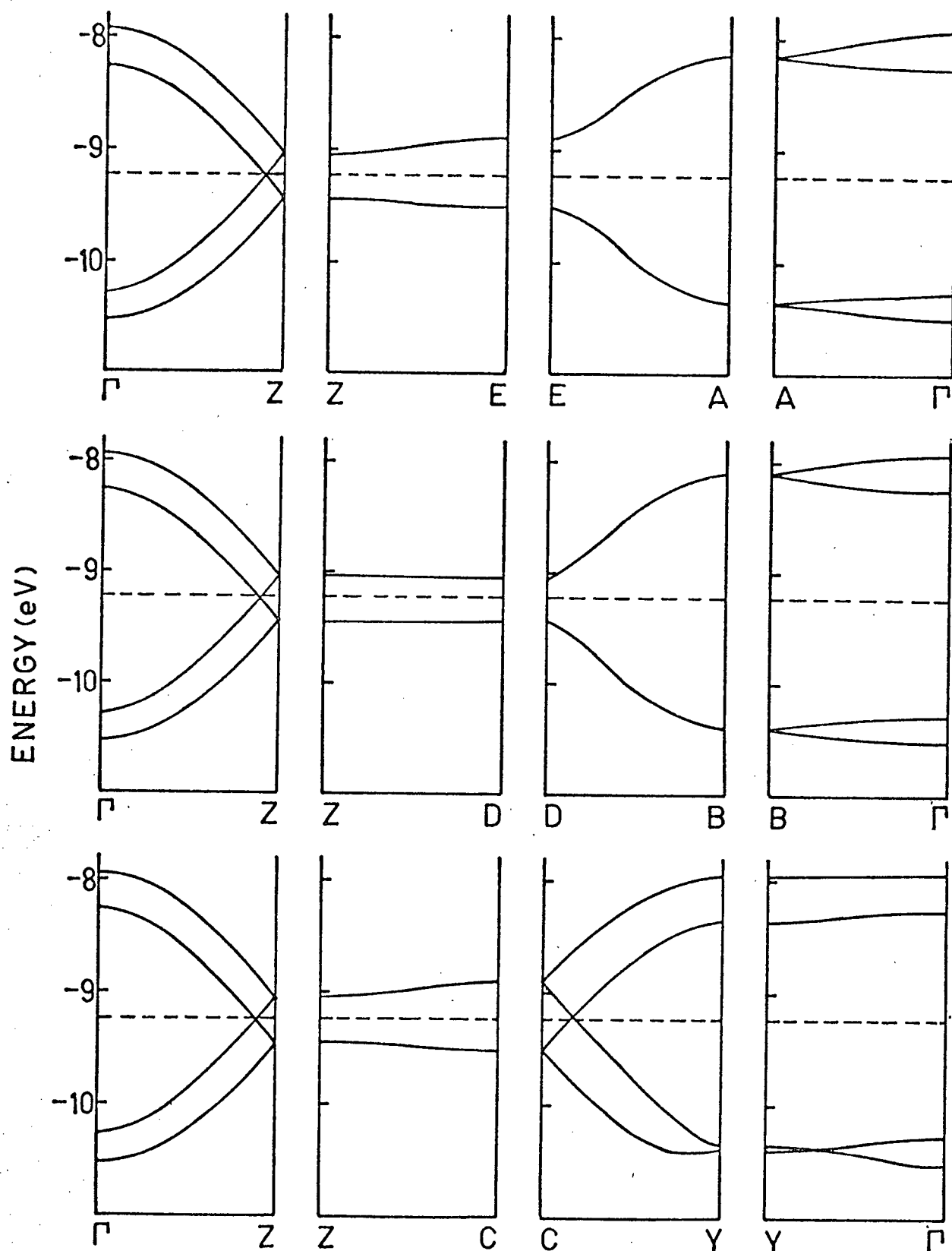
Figure A2. Three-dimensional band structure obtained by the extended
Hückel method incorporating the Penn crystal structure.

is,

$$H = \begin{bmatrix} \alpha & \beta^* & \mu^* & \delta^* \\ \beta & \alpha & \delta^* & \nu^* \\ \mu & \delta & \alpha & \beta^* \\ \delta & \nu & \beta & \alpha \end{bmatrix} \qquad\qquad (A1)$$

The matrix elements are given by,

$$\alpha = 2t_1 \cos \vec{k} \cdot \vec{a}$$
$$\beta = t_2(1 + e^{-i\vec{k}\cdot\vec{b}})$$
$$\mu = t_3 e^{-i\vec{k}\cdot\vec{b}} + t_4 e^{i\vec{k}\cdot(\vec{a}-\vec{b})} \qquad\qquad (A2)$$
$$\nu = t_3 e^{-i\vec{k}\cdot\vec{c}} + t_4 e^{-i\vec{k}\cdot(\vec{a}+\vec{c})}$$
$$\delta = t_5(1 + e^{i\vec{k}\cdot\vec{b}})$$

where the t_i's represent the following interactions:

(i) t_1: a σ-interaction between two S_1 atoms in cells displaced by $\vec{a}$.

(ii) t_2: the interaction between molecules on the same chain.

(iii) t_3: a σ-interaction between an S_1 and the S_3 in the cell translated by $\vec{b}$.

(iv) t_4: a π-interaction between an S_1 and the S_3 in the cell displaced by $\vec{b} - \vec{a}$.

(v) t_5: a σ-interaction between an S_1 and the S_4 in the cell translated by $\vec{c}$.

With the parameters $t_1 = 0.02$ eV, $t_2 = -0.57$ eV, $t_3 = 0.25$ eV, $t_4 = -0.06$ eV, and $t_5 = 0.04$ eV, the energy bands depicted in Fig. A3 again bear a

strong similarity to those in Fig. A2.

The conclusion to be drawn from this calculation incorporating the Penn structure is the same as that of §3.3: (SN)x is a semimetal.

Table A1. Atomic coordinates in the (SN)x unit cell for the Penn structure. In the coordinate system employed, the lattice vectors are, in Å units: $\vec{a}$ = (4.15,0,0), $\vec{b}$ = (0,4.44,0), and $\vec{c}$ = (-2.57,0,7.19).

	X	Y	Z
S_1	-1.143	1.275	1.119
S_2	-0.143	-0.945	2.475
S_3	1.143	-1.275	-1.119
S_4	0.143	0.945	-2.475
N_1	-1.043	-0.307	1.279
N_2	-0.243	-2.526	2.315
N_3	1.043	0.307	-1.279
N_4	0.243	2.526	-2.315
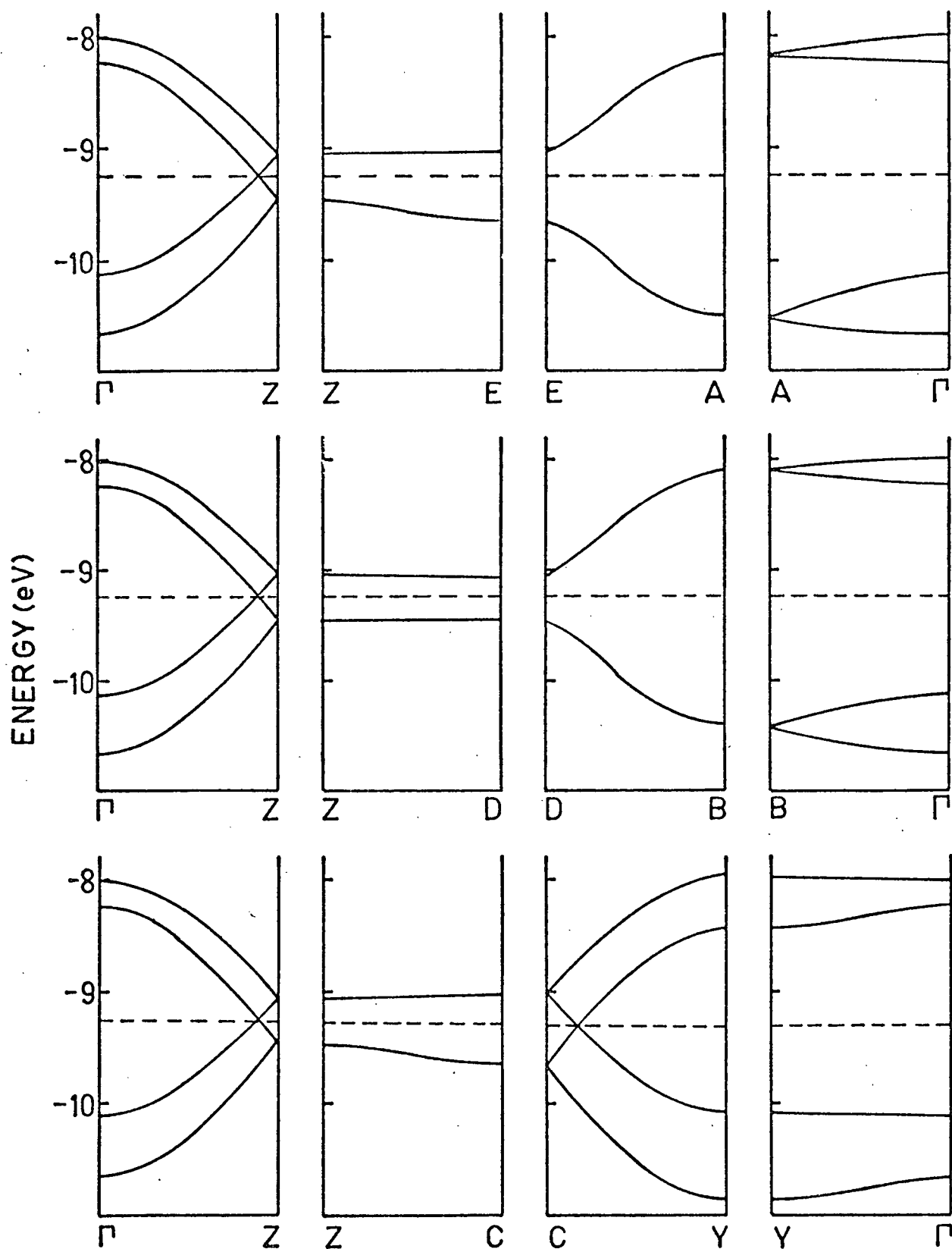
Figure A3. Tight-binding analogue of Fig. A2.